Gut microbiome-based prediction of autoimmune neuroinflammation

Alex Steimle[1,†], Mareike Neumann[1,2,†], Erica T. Grant[1,2], Stéphanie Willieme[1], Alessandro De Sciscio[1], Amy Parrish[1,2], Markus Ollert[1,3], Eiji Miyauchi[4,5], Tomoyoshi Soga[6], Shinji Fukuda[6,7,8,9], Hiroshi Ohno[4] and Mahesh S. Desai[1,3,*]

[1]Department of Infection and Immunity, Luxembourg Institute of Health, L-4354 Esch-sur-Alzette, Luxembourg

[2]Faculty of Science, Technology and Medicine, University of Luxembourg, L-4365 Esch-sur-Alzette, Luxembourg

[3]Department of Dermatology and Allergy Center, Odense Research Center for Anaphylaxis, University of Southern Denmark; DK-5000 Odense, Denmark

[4]RIKEN Center for Integrative Medical Sciences; 1-7-22 Suehiro-cho, Tsurumi-ku, Yokohama City, Kanagawa, 230-0045, Japan

[5]Institute for Molecular and Cellular Regulation, Gunma University, 3-39-15 Showa-machi, Maebashi, Gunma, 371-8512, Japan

[6]Institute for Advanced Biosciences, Keio University, 246-2 Mizukami, Kakuganji, Tsuruoka-shi, Yamagata 997-0052, Japan

[7]Gut Environmental Design Group, Kanagawa Institute of Industrial Science and Technology, 3-25-13 Tonomachi, Kawasaki-ku, Kawasaki, Kanagawa 210-0821, Japan

[8]Transborder Medical Research Center, University of Tsukuba, 1-1-1 Tennodai, Tsukuba-shi, Ibaraki 305-8575, Japan

[9]Laboratory for Regenerative Microbiology, Juntendo University Graduate School of Medicine, 2-1-1 Hongo, Bunkyo-ku, Tokyo 113-8421, Japan

[†]These authors contributed equally

[*]Corresponding author. E-Mail: mahesh.desai@lih.lu

Abstract

Gut commensals are linked to neurodegenerative diseases, yet little is known about causal and functional roles of microbial risk factors in the gut–brain axis. Here, we employed a pre-clinical model of multiple sclerosis in mice harboring distinct complex microbiotas and six defined strain combinations of a functionally-characterized synthetic human microbiota. Discrete microbiota compositions resulted in different probabilities for development of severe autoimmune neuroinflammation. Nevertheless, assessing presence or the relative abundances of a suspected microbial risk factor failed to predict disease courses across different microbiota compositions. Importantly, we found considerable inter-individual disease course variations between mice harboring the same microbiota. Evaluation of multiple microbiome-associated functional characteristics and host immune responses demonstrated that the immunoglobulin A-coating index of *Bacteroides ovatus* before disease onset is a robust individual predictor for disease development. Our study highlights that the "microbial risk factor" concept needs to be seen in the context of a given microbial community network, and host-specific responses to that community must be considered when aiming for predicting disease risk based on microbiota characteristics.

41 **INTRODUCTION**

42 Compared to healthy controls, autoimmune disease patients exhibit distinct microbiota compositions (*1*),
43 especially in the context of multiple sclerosis (MS) (*2*). Thus, determining whether susceptibility or
44 progression of MS can be predicted by the microbiota composition is a necessary precondition to develop
45 patient-targeted microbiota modulations (**Fig. 1a**). A common approach to elucidate microbiota-related, MS-
46 promoting predictors compares relative abundances of bacterial taxa – often determined by 16S rRNA gene-
47 based sequencing – between MS-affected and healthy individuals (*2-9*). Although certain differentially
48 abundant taxa identified across different human cohort studies tend to be concordant, e.g., increased
49 abundances of *Akkermansia* (*2, 4, 5, 7-9*) or decreased abundances of *Prevotella* (*3, 5-8*) in MS patients
50 compared to healthy controls, such cohort-level observations do not explain inter-individual differences (*10*)
51 in disease course or susceptibility. Therefore, it remains challenging to reliably link taxa abundances across
52 individuals to microbiota characteristics that impact MS disease course.

53 Given the limitations of correlation-focused human cohort studies to uncover reliable microbial risk factors
54 for MS susceptibility, the experimental autoimmune encephalomyelitis (EAE) mouse model is commonly used
55 to verify presumed causality between presence of suspected microbial risk factors and development of
56 autoimmune neuroinflammation (*11-13*). However, it is unclear whether the causality of a singular species
57 alone or within only one specific background microbiota, i.e. in mice harboring a relatively consistent, specific
58 pathogen-free (SPF) microbiota composition, can be translateable to the plethora of individual microbiota
59 compositions found across a given population (*1*). Although certain inter-microbial interactions, that promote
60 EAE development, have previously been revealed (*11, 14*), the mutual impact between the background
61 microbiota and potential commensal risk factors on disease-promoting properties of the microbiota is poorly
62 understood.

63 Here, we investigated whether the EAE disease course can be predicted before disease onset by microbiota-
64 associated readouts. For reliable EAE disease prediction, we weighed in microbial taxonomic composition
65 analyses against microbiota-associated, functional analyses, and we investigated the host immune responses.
66 Our comprehensive approach allowed us to examine how individual host−microbe interactions interfere with
67 disease predictability.

68 **RESULTS**

69 ***Muc2*-deficiency in mice is associated with less severe experimental autoimmune encephalomyelitis**

70 During experimental autoimmune encephalomyelitis (EAE), the microbiota composition impacts how the host
71 immune system is shaped (*15*), impacting the degree of neuroinfammation. Investigating how different disease
72 phenotypes could be predicted based on the microbiota composition could be a key toward microbiota-based
73 intervention (**Fig. 1a**). As a first step toward testing our hypothesis, we set out to identify the EAE
74 development-associated commensal genera within a complex microbiota. To do so, we induced EAE in
75 specific pathogen free (SPF) mice of different origins and genotypes. We fed these mice diets with different
76 fiber contents, given the impact of dietary fiber quality and quantity on relative abundances of indigenous
77 commensals (*16, 17*). First, we addressed the question of whether changing relative abundances of taxa within
78 a given microbiota might affect outcome of EAE. Toward this goal, we used wildtype C57BL/6J mice
79 purchased from Charles River (CR), which were fed either a standard laboratory chow (fiber-rich; FR) or a
80 fiber-free diet (FF) diet for 20 days, followed by induction of EAE (**Fig. 1b**). Feeding these diets did not result
81 in different disease outcomes (**Fig. 1c–e**), indicating that dietary fiber quantity and quality, and the associated
82 effects on relative abundances of taxa within this particular indigenous microbiota, are not determining factors
83 in mediating EAE (**Fig. 1f**).

84 Next, we sought to elucidate whether we could observe distinct EAE outcomes between mice whose native
85 microbiota differentiated considerably by the presence of certain taxa, rather than by relative abundances of a
86 shared core microbiota. To do this, we induced EAE in mice deficient for the Muc2 protein ($Muc2^{-/-}$), as this
87 genetic modification results in an impaired mucus barrier (*18*). We expected a significantly different
88 indigenous microbiota composition due to anticipated reduction in commensals relying on an intact mucus
89 layer as a functional or nutritional niche (*19*). As controls, we used littermate mice homozygous for the
90 presence of *Muc2* gene ($Muc2^{+/+}$). While $Muc2^{+/+}$ mice were fed both FR or FF diet, $Muc2^{-/-}$ mice were only
91 fed a FR diet (**Fig. 1g**). We observed a significant difference in disease progression between the genotypes,
92 with $Muc2^{-/-}$ mice being significantly less susceptible to EAE induction compared to $Muc2^{+/+}$ mice, regardless
93 of diet (**Fig. 1h–j**). As observed for CR mice (**Fig. 1f**), diet-mediated influences on disease development were
94 negligeble (**Fig. 1k**).

Higher abundances of *Akkermansia muciniphila* are associated with less severe EAE in mice with a complex microbiota

To evaluate a potential contribution of the microbiota to the observed differences, we performed 16S rRNA gene-based sequencing analyses on DNA isolated from fecal samples taken before EAE induction (**Fig. 1l–m; Extended Data Fig. 1a–f**) and during the EAE course (**Extended Data Fig. 1a–e**). Intriguingly, the overall microbiota β-diversity (**Extended Data Fig. 1a−d**) and α-diversity (**Extended Data Fig. 1e**) were disconnected from the EAE disease course. Since all four groups of mice expressing the Muc2 protein (CR mice and *Muc2*$^{+/+}$ mice) provided a comparable EAE disease course (**Fig. 1c, h**), which was significantly different from the one observed in *Muc2* knockout (KO) mice (**Fig. 1h)**, we assessed potential EAE-relevant microbiota differences by comparing *Muc2*$^{-/-}$ mice (KO) with all *Muc2*-expressing mice combined (WT), irrespective of origin or diet. We identified 11 differentially abundant genera that explained more than 70% of the variance detected in the Bray−Curtis distance matrix between WT and KO mice before induction of EAE (pre-EAE). Pre-EAE relative abundance of the genus *Akkermansia* alone explained 14.4% of said variance (**Fig. 1l,** right panel), correlated negatively with various EAE readouts upon induction of disease (**Fig. 1l** left panel), and was significantly higher in *Muc2*$^{-/-}$ mice compared to WT counterparts (**Fig. 1m**), suggesting possible disease-preventing properties of *Akkermansia*.

However, our observations so far are inadequate to attribute distinct EAE phenoytpes exclusively to changes in *Akkermansia* abundance, or micobiota changes in general, because potential *Muc2* knockout-associated changes in host responses were not specifically addressed. Nonetheless, given that *Akkermansia* is consistently reported as a potential risk factor for MS (*2, 4, 5, 7-9*) and due to its controversial role in EAE development (*2, 20*), we asked whether the observed potential disease-preventing properties in our experiments might be rooted in distinct background microbiota compositions, as *Akkermansia* was embedded in diverse microbiotas with different taxa present or absent (**Extended Data Fig. 1f**).

Removal of *Akkermansia muciniphila* from a synthetic microbiota results in less severe EAE

To better understand a potential causal role of *Akkermansia* in EAE development and to evaluate its potential as a disease-risk predictor, we colonized germ-free (GF) C57BL/6 mice with a functionally-characterized 14-member human synthetic microbiota (SM14) (*16, 21*) (**Fig. 2a**). This approach allowed us to drop out specific

122 species-of-interest from this community to investigate the contribution of a single microbe on EAE
123 development in a genetically homogenous host. *Akkermansia muciniphila*, the type species for the
124 *Akkermansia* genus, is a member of this SM14 community. Thus, we colonized GF C57BL/6 mice with either
125 the complete SM14 community or a SM13 community, lacking *A. muciniphila*, followed by induction of EAE
126 (**Fig. 2b**). SM13-colonized mice exhibited a significantly less severe EAE phenotype compared to SM14-
127 colonized counterparts (**Fig. 2c**, left panel; **Fig. 2d−f**), highlighting the general contribution of the microbiota
128 to EAE development and the disease-driving role of *A. muciniphila* in the SM14 microbiota-based mouse
129 model when this species is combined with the 13 strains listed in **Fig. 2a**. As controls, we induced EAE in *A.*
130 *muciniphila*-monoassociated (SM01) and GF mice (**Extended Data Fig. 2**). SM01-colonized and GF mice
131 provided a low-to-intermediate EAE disease phenotype (**Extended Data Fig S2b−d**).

132 To evaluate whether changes in relative abundances of SM14-constituent strains might affect EAE disease
133 course, we fed SM14- and SM13-colonized mice an FF diet, followed by EAE induction (**Fig. 2b**). GF mice
134 were also fed a FF diet to exclude microbiota-independent but diet-mediated effects on EAE. Feeding SM14-
135 colonized mice the FF diet resulted in significantly increased *A. muciniphila* relative abundances compared to
136 equally colonized FR-fed mice (**Fig. 2g**). However, we did not detect any significant differences in any EAE-
137 associated readout (**Fig. 2c,** right panel; **Fig. 2f**) between FR- and FF-fed mice harboring the same microbiota.
138 Removal of *A. muciniphila* from the SM14 community explained between 22% and 28% of the variance for
139 different EAE-associated readouts (**Fig. 2e, f; Extended Data Fig. 2a,** right panel). Given that SM01-
140 colonized mice only provided an intermediate disease phenotype (**Extended Data Fig. 2b−d**), our results
141 suggest that the presence of *A. muciniphila* represents a potential microbial risk factor for severe EAE when
142 combined with certain other strains (SM14) and that changes in its relative abundance within *A. muciniphila*-
143 containing communities negligibly impact EAE disease course.

144 ***Akkermansia muciniphila*-associated cecal concentrations of γ-amino butyric acid are linked to EAE**
145 **severity**

146 To evaluate how *A. muciniphila* might alter microbiota function (**Fig. 1a**) within the SM14 reference
147 microbiota, we performed metabolomic and metatranscriptomic analyses. EAE is associated with changes in
148 either plasma metabolite profiles (*22, 23*) or changes in metabolic pathways of the intestinal microbiota (*24*).

149 Furthermore, *A. muciniphila* mediates other pathologies, at least in part, via secretion of certain metabolites
150 (*25*). Thus, we asked whether different levels of neuroinflammation between SM14- and SM13-colonized mice
151 could be explained by *A. muciniphila*-associated metabolite patterns in the cecum or serum. In addition to
152 collecting cecal and serum samples from EAE- induced GF, SM01-, SM13- and SM14-colonized mice, we
153 also collected the same samples from the same groups of non-EAE induced mice. The cecal metabolite profiles
154 were similar between EAE-induced and non-EAE induced groups harboring the same microbiota, as well as
155 between EAE-induced SM13-colonized and SM14-colonized mice (**Fig. 3a, b**). As broader metabolic profiles
156 were disconnected from the EAE disease course (**Extended Data Fig. 3a**), we reasoned that only a few cecal
157 metabolites, if any, might causally influence the EAE disease course.

158 To identify such potential EAE-impacting metabolites, we developed a metabolite-of-interest screening
159 pipeline including 20 independent analyses (**Extended Data Fig. 3b−e**). We proposed that a potential *A.*
160 *muciniphila*-associated and disease-mediating metabolite should fulfill five different criteria. The rationale for
161 these criteria and the analytical approach is specified in the Materials and Methods section. Among the 18
162 metabolites that significantly correlated with at least one EAE-associated readout, only γ-amino butyric acid
163 (GABA) emerged as a metabolite-of-interest in cecal samples (**Fig. 3c**). Of note, its concentration was
164 significantly elevated in non-EAE-induced mice harboring an SM combination which resulted in severe EAE
165 upon disease induction. (**Fig. 3d**). Given that GABA concentrations were higher in disease-prone, *A.*
166 *muciniphila*-harboring mice, these results suggested that the cecal concentration of GABA before EAE
167 induction already defined disease development upon disease induction and that its concentration was linked to
168 disease-influencing properties of the tested microbial communities harboring *A. muciniphila*. Additionally, we
169 did not identify any metabolite-of-interest in serum samples (analyses not shown), indicating that potential
170 metabolite-driven impacts on EAE disease course occur locally in the intestine.

171 **Presence of *Akkermansia muciniphila* significantly alters gene expression profiles of other microbial**
172 **community members**

173 Given these community-dependent alterations in microbial metabolite profiles, we rationalized that the
174 presence or absence of *A. muciniphila* had a significant impact on gene expression profiles of the overall
175 microbiota, possibly contributing to distinct EAE phenotypes. Thus, we performed metatranscriptomic

176 analysis of cecal contents obtained from non EAE-induced SM14- and SM13-colonized mice (**Fig. 3e−g**).
177 When comparing transcript profiles of both groups, we found 117 genes expressed only in SM14-colonized
178 mice (**Fig. 3f**). Although we expected that these transcripts would be mostly from *A. muciniphila*, in fact, most
179 of these genes were exclusively expressed by either *Roseburia intestinalis* or *Marvinbryantia formatexigens*
180 (**Fig. 3g**). Of the 30 genes expressed only in SM13-colonized mice, the majority were expressed by
181 *Eubacterium rectale* (**Fig. 3g**). These findings highlight the crucial impact of the presence of a single
182 commensal on the gene expression pattern of other microbial community members, likely impacting their
183 "function" (**Fig. 1a)** within a given community. These indirect influences on community function might also
184 contribute to microbiota-mediated effects on EAE development and thus impact disease-mediating properties
185 of potential risk-predicting species.

186 **Mucin-degrading capacity of the microbiota is not linked to EAE severity**

187 So far, our results suggest that predicting EAE development, based on the presence or absence of *A.*
188 *muciniphila*, a mucin-specialist bacterium (*16*), was only possible in mice harboring a variation of the SM14
189 community (**Figs. 2, 3**) and not in mice harboring a complex community (**Fig. 1**). To further address potential
190 reasons for these discrepancies in general, and the apparent crucial impact of the presence of *A. muciniphila*
191 in SM14-colonized mice in particular, we next hypothesized that changes in relative abundances of other
192 strains in response to dropping out *A. muciniphila* from the SM14 community might causally impact EAE
193 development. We observed that four strains were significantly higher in abundance in SM13-colonized mice
194 compared to SM14-colonized mice (**Fig. 4a**). To address their potential contribution to EAE development, we
195 colonized mice with three additional SM combinations (**Fig. 4b, Extended Data Fig. 4a**). In the first of these
196 combinations, we colonized GF mice with an SM12 community (**Fig. 4b**), lacking *A. muciniphila* and
197 *Faecalibacterium prausnitzii*. This experiment was performed to elucidate whether the >1000-fold increase in
198 relative abundance of *F. prausnitzii* (**Fig. 4a**, extreme right panel) — a species known for gut health-promoting
199 properties (*26*) and decreased abundances in MS patients (*10*) — in mice lacking *A. muciniphila* (**Fig. 4a**) was
200 responsible for EAE-preventing properties of the SM13 community. Intriguingly, SM12-colonized mice (**Fig.**
201 **4c−e**) provided a comparable disease course as SM13-colonized mice (**Fig. 2**), suggesting that *F. prausnitzii*
202 expansion in SM13-colonized mice is not responsible for decreased EAE in SM13-colonized mice. At the

203 same time, these data point out the *A. muciniphila*-mediated inhibitory effects on the expansion of an anti-
204 inflammatory bacterium, *F. prausnitzii*.

205 Removal of *A. muciniphila* from the SM14 community further resulted in expansion of three mucin glycan-
206 degrading (*16*) Bacteroidetes species (**Fig. 4a**) in the SM13 community. Thus, we investigated whether
207 colonization with the three mucin glycan-degrading strains alone (SM03) resulted in decreased EAE compared
208 to SM14-colonized mice and whether addition of *A. muciniphila* (SM04) might counteract a potential
209 beneficial effect. While SM03- and SM04-colonized mice showed comparable EAE disease courses (**Fig.**
210 **4c−e**) to SM14-colonized mice (**Fig. 2**), they differed significantly from SM13-colonized mice. Additionally,
211 the three mucin glycan-degrading Bacteroidetes strains appeared to not provide disease-reducing properties
212 but, on the contrary, disease-promoting properties in the absence of the remaining 10 strains within the SM13
213 community. To evaluate whether dysregulated mucin turnover might contribute to the observed results in these
214 mice, we assessed various indirect measures for intestinal barrier integrity. We did not detect any correlations
215 between EAE outcome and glycan-degrading enzymatic activities (**Extended Data Fig. 4b−g**), serum
216 concentrations of LPS, occludin or zonulin as well as with fecal concentrations of lipocalin (**Extended Data**
217 **Fig. 4h,i**), or SCFA (**Extended Data Fig. 4j**). Thus, our results suggest that bacterially-mediated mucus glycan
218 degradation or barrier integrity impairment, in the context of the microbiota combinations used in this study,
219 were not an individual predictor for EAE disease development.

220 **Microbiota composition can be used to estimate the probability of severe EAE incidence**

221 Thus far, groupwise comparisons of EAE-associated readouts and microbiota compositions failed to identify
222 reliable predictors for disease development in EAE-induced mice. Therefore, we next aimed to elucidate
223 common denominators on a group-based and individual level to help uncover more reliable potential predictors
224 for microbiota-mediated impacts on disease course. First, we conducted group-based comparison of EAE
225 outcomes between all 10 tested diet−colonization combinations ("groups") (**Fig. 5a, b**). Performing
226 hierarchical clustering (**Fig. 5c**) based on group means of key EAE-associated readouts (**Fig. 5b**) revealed
227 three distinct group phenotypes: "moderate", "intermediate" and "severe". While diet explained less than 8%
228 of the variance observed for EAE-associated readouts, microbiota composition (SM) explained between 11%
229 and 27% (**Fig. 5d**). Given these low values, rooted in considerable intra-group variances (**Fig. 5b**), we

230 performed individual EAE phenotype clustering, treating all mice across all groups individually (**Fig. 5e**). T-
231 distributed stochastic neighbor embedding (t-SNE) analysis of all EAE-induced individuals resulted in two
232 disease clusters: "Cluster 1", comprising mice showing strong EAE symptoms, and "Cluster 2", comprising
233 mice showing minor EAE symptoms (**Fig. 5e**). Besides SM03- and SM04-colonized mice, every group
234 included mice of both phenotypes (**Fig. 5f**), however with varying proportions. These proportions broadly, but
235 not completely, corresponded to the group-based phenotype classification (**Fig. 5c**). In summary, these results
236 (**Fig. 5a−f**) indicate that knowing the composition of the microbiota, in combination with information on
237 dietary conditions, enables estimation of the probability for either moderate or severe disease, but is unsuitable
238 to predict individual EAE outcomes.

239 Given that IL-17- and IFNγ-producing $CD4^+$ cells (*11*), $CD8^+$ cells (*27*), and IgA^+ IL-10^+ plasma cells (*28*) are
240 reported to link the microbiota with EAE development, host-specific influences on these immune responses
241 might contribute to individually different disease outcomes despite identical microbiome compositions.
242 Examining such effects in more detail is critical for making disease course predictions based on microbiota
243 composition or function. Thus, we analyzed T and B cell polarization in mice before and after EAE induction
244 to elucidate whether potential host-specific responses occurred upstream or downstream of immune cell
245 activation. While we detected no differences in B cell subsets among EAE-induced mice, we found 25 T cell
246 populations in four different organs with significantly different relative abundances between groups (**Fig. 5g**,
247 left panel; **Extended Data Fig. 5a**). Among those, nine populations also correlated with individual outcome
248 of EAE (**Fig. 5g,** left panel). Among all tested organs (colonic and ileal lamina propria, mesenteric lymph
249 nodes and spinal cords), relative abundances of T cell populations in the spinal cords corresponded best, but
250 not perfectly, to the respective EAE group phenotype (**Fig. 5g**, right panel). While group-wise comparison of
251 each T cell population failed to explain observed EAE phenotypes, individual cluster-based analyses
252 (**Extended Data Fig. 5e**) showed significant differences for seven populations, with IFNγ-expressing Th17
253 cells in the spinal cords significantly increased in Cluster 1-mice (**Fig. 5h**). Mouse-specific T cell polarization
254 profiles aligned better with disease outcome (**Fig. 5h**) than with SM−diet combinations (**Fig. 5h**). Thus, we
255 concluded that host-specific differences must occur before T cell activation in EAE-induced mice, most

256 probably due to individual microbiota-mediated signals that appeared to be distinct even in mice harboring the
257 same set of strains.

258 When analyzing T cell subsets in non-EAE induced mice, we found that the microbiota composition primed
259 $CD4^+$ T cells towards a pro-inflammatory Th17 response before EAE-induction (**Extended Data Fig. 5b**).
260 Although we found more significant correlations of these populations with EAE-associated readouts in the
261 ileum, overall T cell population distribution in the colon aligned best with emerging EAE group phenotypes
262 upon EAE induction (**Extended Data Fig. 5c,d**), suggesting a crucial contribution of T cell priming in the
263 colon by the microbiota to disease development upon EAE induction.

264 In summary, it was impossible to predict individual disease development based on microbiota−diet
265 combinations alone despite apparent microbiota-mediated priming of the local adaptive immune system before
266 EAE induction. This observation suggests that microbiota-mediated signals that influence the adaptive immune
267 system to either promote or decelerate EAE development are relatively constant before disease induction, but
268 are prone to individual changes upon disease onset.

269 **IgA coating index of *Bacteroides ovatus* represents a surrogate measure to predict microbiota-mediated**
270 **impact on individual EAE severity**

271 Considering these individual signaling changes, we next targeted identification of microbiota-associated
272 factors suitable to predict individual outcome of EAE. For each given strain (**Fig. 6a**), we first assessed whether
273 its relative abundance before EAE induction (**Extended Data Fig. 6a**), as determined by 16S rRNA gene
274 sequencing in each individual mouse, allowed for prediction of individual disease course after EAE induction
275 (**Fig. 6b, c**). To do so, we only included mice harboring at least 12 different strains, thus excluding mice with
276 low-diversity microbiotas (SM04, SM03, SM01). Correlations for each strain were only assessed for those
277 mice, which were gavaged with the respective strain and calculations were performed by either including mice
278 harboring SM14, SM13 and SM12 communities, or specific combinations thereof, into the analysis. We found
279 statistically significant correlations between pre-EAE bacterial relative abundances with EAE-associated
280 readouts for some strains (**Fig. 6b)**. However, the few statistically significant correlations we determined were
281 generally weak ($R<0.4$) and Pearson correlation values for a given strain were highly dependent on the

282 background microbiota (**Fig. 6b)**. In line with this, relative abundances of strains only explained very low
283 proportions of the variances across all groups for all assessed EAE-associated readouts (**Fig. 6c**).

284 Next, we asked whether presence or absence of a given strain might be a better predictor for individual EAE
285 development. Thus, we performed a linear mixed model regression for three EAE-associated readouts with
286 presence of the strain as an independent variable and colonization as a random intercept effect (**Fig. 6d**,
287 **Extended Data Fig. 6b**). Given the setup of our tested SM-combinations, we could only assess *A. muciniphila*
288 and *F. prausnitzii* separately and had to analyze the remaining 12 strains in groups of two combinations.
289 Presence or absence of a specific strain or strain combination was insufficient to predict the individual outcome
290 of any of the tested EAE-associated readouts (**Fig. 6d, Extended Data Fig. 6b**), indicating that potential
291 disease-driving or -preventing properties of a given strain or strain combination is crucially determined by the
292 background microbiota.

293 Coating of intestinal commensals by host plasma cell-derived IgA represents a crucial host response for
294 maintaining immune homeostasis in the context of autoimmune neuroinflammation (*29-31*). Secretory IgA
295 (sIgA) levels in the mouse feces were disconnected from individual EAE outcomes (**Extended Data Fig. 6c**),
296 but were strongly connected to the microbiota composition (**Extended Data Fig. 6d**). Interestingly, we found
297 a significant correlation between group means of sIgA concentrations and corresponding EAE susceptibility
298 incidence (**Extended Data Fig. 6e**). Owing to these observations and given that the "IgA-coating index" (ICI)
299 was previously suggested to be a measure of autoimmunity-promoting potential of a given commensal species
300 (*32*), we determined ICIs for each strain within each high-diversity SM combination (SM12, SM13 and SM14)
301 in every individual (**Fig. 6e−g, Extended Data Fig. 6f−h**). Interestingly, there was a tendency for ICIs to differ
302 between distinct SM-combinations **(Extended Data Fig. 6f)** and microbiota composition explained more than
303 40% of the variance between ICIs of *B. ovatus* and *B. uniformis* **(Fig. 6e, Extended Data Fig. 6g)**, suggesting
304 a crucial role of the background microbiota on strain-specific IgA coating (**Extended Data Fig. 6h)**.
305 Additionally, ICIs of these strains varied not only between distinct groups, but also between individuals within
306 groups. Thus, we reasoned that the individual ICI of these strains might reflect individual EAE-promoting
307 properties of the microbiota in a certain host. Correlation analysis of strain-specific ICI, as determined from
308 fecal samples obtained before EAE induction, with EAE outcome in the same individual, revealed significant

309 correlations with some EAE-associated readouts for four strains (**Fig. 6f**). However, the only strain whose
310 individual ICI provided significant correlations with the two most important EAE-associated readouts (AUC
311 and maximum achieved EAE score) was *B. ovatus* (**Fig. 6f, g**), thus allowing for individual prediction of EAE
312 disease course across all *B. ovatus*-encompassing SM combinations (**Fig. 6g**).

313 **DISCUSSION**

314 Given the association between the intestinal microbiota and extra-intestinal autoimmune diseases (*1*),
315 microbiota manipulation is a feasible approach to boost existing therapy options for MS patients. Potential
316 strategies for microbiota modulation include administration of antibiotics or probiotics (*33*), dietary
317 interventions (*34, 35*) or fecal microbiota transplantation (*36*). However, such untargeted strategies could lead
318 to broad-scale changes in the microbiota with potentially unpredictable outcomes. On the contrary, given the
319 unique microbiota composition in a given individual, personalized approaches might be more promising.

320 A better understanding of what exactly makes a specific microbiota composition in a given individual disease
321 prone is a precondition for a targeted personalized approach. Such knowledge is expected to result in analytical
322 procedures to evaluate the average risk of disease or even predict individual outcomes. Previously suggested
323 measures to evaluate the MS-mediating risk of a microbial community, such as the microbiota α-diversity (*37*)
324 or the Firmicutes-to-Bacteroidetes ratio (*38*), emerged as unsuitable tools (*10*) and more focus is currently
325 being put on individual taxa or combinations of taxa (*10*). A recent mouse study suggested that up to 50
326 different microbial taxa could be associated with disease (*39*). Disease-associated bacterial taxa are often
327 referred to as "microbial risk factors", which are mostly identified by differences in presence or relative
328 abundances from cross-sectional human cohort studies. *Akkermansia muciniphila* represents such a potential
329 microbial risk factor as it was reportedly increased in MS patients across various human cohorts (*2, 5, 7, 40*).
330 Other studies, however, report on positive effects of *A. muciniphila* on maintaining general gut homeostasis
331 (*41, 42*) or on progression of autoimmune neuroinflammation in mice (*20*).

332 At first sight, these observations might appear contradictory. They are, however, corroborated by our findings.
333 By comparing development of experimental autoimmune encephalomyelitis (EAE) in mice of different genetic
334 backgrounds and with distinct complex microbiotas, we found the genus *Akkermansia* to be the most
335 negatively associated with EAE disease development, thus representing a potential hallmark genus for less
336 severe EAE, when considering the microbiota composition as the only variable and ignoring host genetics
337 **(Extended Data Fig. 7)**. Next, we evaluated whether this finding could be reproduced in gnotobiotic,
338 genetically homogenous mice harboring different combinations of a reduced reference microbiota, with or
339 without *A. muciniphila*. Interestingly, we found *A. muciniphila* to be positively associated with EAE severity

340 in certain mice harboring specific reduced communities. This was associated with increased cecal levels of γ-
341 amino butyric acid (GABA). However, we cannot reliably conclude whether increased GABA concentrations
342 are a general risk factor for EAE induction or whether this only applies to a certain microbiota composition.
343 Since elevated GABA levels were previously reported to be associated with less neuroinflammation (*43, 44*),
344 we deemed assessment of intestinal GABA concentration, without corresponding information on microbiota
345 composition, unsuitable for disease course prediction. It is unclear whether this neurotransmitter directly
346 mediates EAE-influencing host responses via interaction with local host receptors (*45*) or whether it might act
347 as a signaling molecule or energy source (*46*) for other species, which finally mediate disease promotion.

348 Our study suggests that focusing on microbiota composition only, as we did in our experiments using mice of
349 different genotypes, can result in misleading conclusions. Co-variates, such as diet, sex, medication use,
350 geographic location, disease subtypes and genetic heterogeneity of study participants make interpretation of
351 microbiota data from human cohort studies complicated, although certain biostatistic approaches help to
352 reduce the risk of misinterpretation, as elegantly shown in a recent publication from the iMSMS Consortium
353 (*10*). In addition, we found that 16S rRNA gene sequencing-based determination of relative taxa abundances
354 is unsuitable to make meaningful assumptions on disease-mediating properties of a given microbiome.
355 Assessing the presence or absence of taxa allowed us to determine the probability of severe disease (**Fig. 6h**:
356 "Risk of disease"). However, this observation was unrelated to presence or absence of a single taxon,
357 suggesting that focusing on combinations of taxa and/or environmental factors, rather than single taxa alone,
358 may be required to form reliable conclusions. Thus, our results suggest that mutual influences between a
359 suspected risk factor and the microbial environment crucially shape the overall microbiota's disease-impacting
360 potential **(Extended Data Figure 7)**.

361 Our metatranscriptomics analyses revealed that even minor changes in microbiota composition, i.e. by
362 removing *A. muciniphila* from a reduced community, resulted in profound changes in gene expression patterns
363 of some, but not all, intestinal microbes. Such influences may also affect disease-mediating properties of the
364 microbiota. Therefore, we suggest to put more focus on microbial network analysis to disentangle specific
365 inter-microbial interactions. Although not yet a technically and analytically refined approach (*47*),
366 metagenomic-based microbiota network analyses are currently being explored as an analysis tool (*48*) and

367 might be superior to statistical analysis of species−species co-abundances (*10*). A key study, evaluating the
368 effects of multiple defined microbiota compositions on fitness of *Drosophila melanogaster*, already pointed
369 out that microbial network interactions are more important than relative abundances of a given species alone
370 (*49*). Our study documents similar innovative findings, based on comprehensive datasets, in a controlled
371 vertebrate gnotobiotic disease model..

372 In addition to these microbiota-specific effects, host-specific effects appeared to be a decisive factor for
373 individual EAE development in our experiments, further complicating the quest for reliable disease predictors.
374 Even in genetically homogenous mice of the same sex and age, harboring the exact same set of commensal
375 bacteria and living under the same standardized conditions, we found considerable individual differences in
376 EAE disease course, suggesting that the individual disease development is mediated by either
377 microbe−microbe or microbe−host interactions (*50, 51*) (**Fig. 6h**). After extensive evaluation of multiple
378 microbiota-associated readouts, we found the IgA-coating index (ICI) of the fiber-degrader *Bacteroides ovatus*
379 *(16)* to be capable of sensing the individual EAE-influencing properties of the microbiota, irrespective of its
380 definite composition. Determining the ICI of *B. ovatus* before disease induction correctly predicted EAE
381 outcome in every individual (**Fig 6h**: "Prediction of disease"). Thus, we propose that *B. ovatus* acts as a
382 "reporter species", reflecting the individual microbiota- and host-mediated dual influences on EAE progression
383 while taking into account distinct microbiota functions across different hosts (**Fig. 6h**: "host-mediated effects
384 on Function"). In the current study, although such a property of *B. ovatus* was only evaluated in reduced
385 microbial communities, the concept of "reporter species" might also apply to other strains and more complex
386 communities, including MS patient microbiotas. A recent study showed that different strains of *B. ovatus* are
387 capable of driving variable host IgA secretion (*52*), which might also impact the IgA coating of *B. ovatus*.
388 Although we did not evaluate in our study whether different strains of *B. ovatus* evolve in different mice, future
389 studies need to consider such aspects.

390 In summary, we demonstrate that making disease-course predictions based on microbiota characteristics is
391 generally possible, but is not as black-and-white as it might appear. We therefore strongly argue for a
392 reconsideration of how microbiota-related data are analyzed and interpreted. In particular, we advocate for

393 higher analytical standards, with more sophisticated data integration to better account for discrepancies in host-

394 specific microbiota function.

395 **MATERIALS AND METHODS**

396 **Institutional Review Board Statement for conduction of mouse experiments**

397 All mouse experiments followed a two-step animal protocol approval procedure. Protocols were first evaluated
398 and pre-approved by either the ethical committee of the University of Luxembourg (AEEC) or the Animal
399 Welfare System (AWS) of the Luxembourg Institute of Health, followed by final approval by the
400 Luxembourgish Ministry of Agriculture, Viticulture, and Rural Development (Protocol numbers:
401 LUPA2020/02, LUPA2020/27, LUPA2020/32, LUPA2019/43, LUPA2020/22, LUPA2019/51) before start of
402 experiments. All experiments were performed according to the Federation of European Laboratory Animal
403 Science Association (FELASA). The study was conducted according to the "Règlement grand-ducal du 11
404 Janvier 2013 relatif à la protection des Animaux utilisés à des fins Scientifiques" based on the "Directive
405 2010/63/EU" of the European Parliament and the European Council from September 2010 on the protection
406 of animals used for scientific purposes. All animals were exposed to 12 hours of light daily.

407 **Origin of mice and housing conditions**

408 For gnotobiotic experiments, female germ-free (GF) C57BL/6N mice were purchased from Taconic
409 Biosciences, USA, at the age of 4 to 8 weeks. All animals were housed and bred in the GF facility of the
410 University of Luxembourg, supervised by the ethical committee of the University of Luxembourg (AEEC).
411 Mice were randomly allocated to different experimental groups and were housed in ISO-cages in groups with
412 a maximum of five animals per cage. Water and diets were provided ad libitum. Before start of experiments,
413 GF status of all mice was confirmed via anaerobic and aerobic incubation of fecal samples in 5 ml culture
414 tubes containing two different rich media, Brain Heart Infusion Broth and Nutrient Broth.

415 For experiments performed under specific pathogen-free (SPF) conditions, as shown in Fig. 1, we used female
416 mice of different origin. C57BL/6J wildtype mice were purchased from Charles River at the age of 5 to 8
417 weeks. Furthermore, we used mice lacking the *Muc2* gene (strain designation: 129P2/OlaHsd×C57BL/6-
418 Muc2<tm1Avel>), which were originally obtained from University of Bern, Switzerland under GF conditions.
419 GF 129P2/OlaHsd×C57BL/6-Muc2<tm1Avel> mice were mated with SPF-housed C57BL/6 mice obtained
420 from Charles River resulting in offspring heterozygous for presence of the *Muc2* gene ($Muc2^{+/-}$). $Muc2^{+/-}$ mice
421 were constantly kept under the same SPF conditions, as the SPF-housed parental C57BL/6 mice. Next, male

422 and female *Muc2*$^{+/-}$ mice were mated and offsprings were genotyped for absence and presence of the *Muc2*
423 gene. Homozygous *Muc2*$^{-/-}$ and *Muc2*$^{+/+}$ mice obtained from this breeding were then used for experiments.

424 **Genotyping for presence or absence of the *Muc2* gene**

425 Genotyping for presence or absence of the *Muc2* gene from mouse ear tissue was performed using the
426 SampleIN™ Direct PCR Kit (HighQu, #DPS0105) according to the manufacturer's instructions. Three
427 different primers were used at a final concentration of 0.4 µM in the PCR reaction (Primer sequences, 5'→3';
428 Primer 1: TCCACATTATCACCTTGAC; Primer 2: GGATTGGGAAGACAATAG; Primer 3:
429 AGGGAATCGGTAGACATC). The PCR was conducted with an annealing temperature of 56 °C and 37
430 cycles. Presence of the *Muc2* gene resulted in an amplificate of 280 bp, while absence of the *Muc2* gene
431 resulted in an amplificate of 320 bp. Amplificates were visualized on a 1.5% agarose gel by gel electrophoresis.

432 **Colonization of germ-free mice with a reduced human synthetic microbiota**

433 All 14 bacterial strains of the synthetic microbiota (SM) were cultured and processed under anaerobic
434 conditions using a Type B vinyl anaerobic chamber from LabGene, Switzerland, as published in detail
435 previously (*21*). A total of six different SM combinations were used to colonize GF mice. Non-colonized GF
436 mice were used as a control group. Intragastric gavage and verification of proper colonization of administered
437 strains was performed as described in detail elsewhere (*21*). Details on the 14 different used strains are
438 summarized in **Extended Data Table 1**.

439 **Mouse diets**

440 Mice were either maintained on a standard mouse chow (fiber-rich; "FR") or switched to a fiber-free ("FF")
441 diet. We used two different FR diets with approximately 15% dietary fiber: SAFE A04 chow (Augy, France,
442 product code U8233G10R) for gnotobiotic mice, sterilized by 25 kGy gamma irradiation, and SDS Standard
443 CRM (P) Rat and Mouse Breeder and Grower diet (Special Diets Service; Essex, UK; product code 801722),
444 sterilized by 9 kGy gamma irradiation, for SPF-housed mice. The FF diet was used for both gnotobiotic and
445 SPF-housed mice and was custom-manufactured by SAFE (Augy, France), based on a modified version of the
446 Harlan TD.08810 diet, as described previously (*53*).

447 **Experimental timeline of mouse experiments**

448 *Experiments performed under gnotobiotic conditions*: At the age of 4 to 8 weeks, mice were colonized with
449 various SM combination (see above), being fed an FR diet. 5 days after initial colonization, mice were either
450 maintained on an FR diet or switched to an FF diet until the end of experiment. Mice were then either induced
451 with experimental autoimmune encephalomyelitis (labelled as "¨+EAE" in the manuscript) 20 days after the
452 initial gavage or were euthanized for organ harvest 25 days after the initial gavage without induction of
453 experimental autoimmune encephalomyelitis (labelled as "¨−EAE" in the manuscript). *Experiments performed*
454 *under SPF conditions*: Mice of all genotypes were raised and maintained on an FR diet. At the age of 6 weeks,
455 mice were either switched to an FF diet or kept on the FR diet. 20 days later, mice fed either diet were subjected
456 to induction of experimental autoimmune encephalomyelitis (EAE). Course of EAE under both, gnotobiotic
457 or SPF, conditions was observed for 30 days.

458 **Experimental autoimmune encephalomyelitis (EAE)**

459 Mice were immunized using the Hooke Kit™ MOG_{35-55}/CFA Emulsion PTX (Hooke Laboratories, #EK-2110)
460 according to manufacturer's instructions. In brief, mice were immunized with a subcutaneous injection of a
461 myelin oligodendrocyte glycoprotein-derived peptide (MOG_{35-55}) and complete Freund's adjuvant (CFA)
462 delivered in pre-filled syringes. Subcutaneous injection of two times 100 µL (200 µL in total) of MOG/CFA
463 (1 mg mL^{-1} MOG_{35-55} and 2-5 mg mL^{-1} killed mycobacterium tuberculosis H37Ra/mL (CFU)) mixture was
464 performed on two sides bilateral in each of the mouse's flank. Additionally, Pertussis toxin (PTX) solution
465 was injected on the day of MOG peptide immunization and 48 hours after the first injection. Glycerol-buffer
466 stabilized PTX was diluted in sterile PBS for application of 400 ng PTX (gnotobiotic experiments) or 150 ng
467 (experiments performed under SPF conditions) by intraperitoneal injection of 100 µL PTX solution. The EAE
468 clinical symptom scores were assessed daily according to the scheme depicted in **Extended Data Figure 8**.
469 For EAE scoring, names of synthetic microbiota groups (such as SM14, SM13, etc.) were blinded. EAE
470 scoring was performed blinded by one researcher (Alex Steimle) and independently unblinded (for microbiota
471 groups) by another researcher (Mareike Neumann), but at the same time. In case of discrepancy of assigned
472 scores by two researchers, the scoring persons discussed and agreed on a certain score. Note that the
473 discrepancy in scoring the same mouse by 2 persons was uncommon due to the rigorous and straight-forward
474 scoring approach outlined in Extended Data Figure 8. If discrepancy happened, the discrepancy was for a max

475 difference of 0.5 score. During EAE scoring, proper care was taken to avoid potential contamination of the
476 gnotobiotic mice.

477 **Euthanisia and organ harvest**

478 Mice of all groups ("− EAE" and "+ EAE") were subjected to terminal anesthesia through intraperitoneal
479 application of a combination of midazolam (5 mg kg^{-1}), ketamine (100 mg kg^{-1}), and xylazine (10 mg kg^{-1})
480 followed by cardiac perfusion with ice-cold PBS. Colonic content, cecal content, blood, and organs were
481 harvested for downstream analysis. Mesenteric lymph nodes (MLN) were removed and homogenized by
482 mechanical passage through a 70 µm cell strainer. MLN cells were washed once in ice-cold PBS for 10 min
483 at 800 × g, resuspended in ice-cold PBS and stored on ice until further use. Colon, ileum were removed and
484 temporarily stored in modified HBSS ("HBSS (w/o)"; Hank's balanced salt solution buffered without Ca^{2+}
485 and Mg^{2+}, buffered with 10 mM HEPES) on ice, while removed spinal cords were temporarily stored in D-
486 PBS. All three organs were then subjected to lymphocyte extraction as decribed below.

487 **Lymphocyte extraction from colonic lamina propria, ileal lamina propria and spinal cords**

488 After organ removal, lymphocytes from the colonic lamina propria (CLP), ileal lamina propria (ILP) and spinal
489 cords (SC) were extracted. While CLP and ILP lymphocytes were extracted using the lamina propria
490 dissociation kit (Miltenyi Biotec, #130-097-410), SC lymphocytes were extracted using a brain dissociation
491 kit (Miltenyi Biotec, #130-107-677), according to the manufacturer's instructions. In brief, colon and ileum
492 were dissected and stored in HBSS (w/o). Feces and fat tissue were removed, organs were opened
493 longitudinally, washed in HBSS (w/o), and cut laterally into 0.5 cm long pieces. Tissue pieces were transferred
494 into 20 mL of a predigestion solution (HBSS (w/o), 5 mM EDTA, 5% fetal bovine serum (FBS), 1 mM
495 dithiothreitol) and kept for 20 min at 37 °C under continuous rotation. Samples were then vortexed for 10 sec
496 and applied on a 100 µm cell strainer. Last two steps were repeated once. Tissue pieces were then transferred
497 into HBSS (w/o) and kept for 20 min at 37 °C under continuous rotation. After 10 seconds of vortexing, tissue
498 pieces were applied on a 100 µm cell strainer. Tissue pieces were then transferred to a GentleMACS C Tube
499 (Miltenyi Biotec, #130-093-237) containing 2.35 mL of a digestion solution and homogenized on a
500 GentleMACS Octo Dissociator (Miltenyi Biotec, #130-096-427, program 37C_m_LPDK_1). Homogenates
501 were resuspended in 5 mL PB Buffer (phosphate-buffered saline (PBS), pH 7.2, with 0.5 % bovine serum

502 albumin), passed through a 70 µm cell strainer and centrifuged at 300 × g for 10 min at 4 °C. Cell pellets were
503 resuspended in ice-cold PB buffer and stored on ice until further use. Spinal cords were stored in ice-cold D-
504 PBS (Dulbecco's phosphate-buffered saline with calcium) until they were transferred to a GentleMACS C
505 Tube containing a digestion solution. Samples were processed on a GentleMACS Octo Dissociator (program
506 37C_ABDK_01) and rinsed through a 70 µm cell strainer. The cell suspension flowthrough was then
507 centrifuged at 300 × g for 10 min at 4 °C. Debris removal was performed by resuspending the cell pellet in
508 1550 µL D-PBS, adding 450 µL of Debris Removal Solution, and overlaying with 2 mL of D-PBS. Samples
509 were centrifuged at 4 °C at 3000 × g for 10 min. The two top phases were aspirated and the cell suspension
510 was diluted with cold D-PBS. Samples were then inverted three times and centrifuged at 4 °C, 1000 × g for 10
511 min and the cell were resuspended and stored in ice-cold D-PBS until further use.

512 **Cell stimulation and flow cytometry**

513 10^6 cells (MLN cell suspensions as well as lymphocyte extracts from CLP, ILP and SC) were resuspended in
514 1 mL complete cell culture medium (RPMI containing 10% FBS, 2 mM Glutamine, 50 U × mL^{-1} penicillin,
515 50 µg × mL^{-1} streptomycin, and 0.1% mercaptoethanol) supplemented with 2 µL Cell Activation Cocktail with
516 Brefeldin A (Biolegend, #423304) and incubated for 4 h at 37 °C. Cells were centrifuged at 500 × g for 5 min,
517 resuspended in 100 µL Zombie NIR (1:1000 in PBS, Zombie NIR™ Fixable Viability Kit, Biolegend,
518 #423106), transferred into a 96-well plate and incubated for 20 min at 4 °C in the dark. Cells were washed two
519 times with 150 µL PBS (centrifuged 5 min at 400 × g at 4 °C) and resuspended in 50 µL Fc-block (1:50,
520 Purified Rat Anti-Mouse CD16/CD32, BD, #553142) diluted in FACS buffer (1x PBS/2% FBS/2mM, EDTA
521 pH 8.0). Cells were incubated for 20 min at 4 °C in the dark and washed two times with 150 µl PBS (centrifuged
522 5 min at 400 × g at 4 °C). All cells were fixed for 30 min with BD Cytofix/Cytoperm solution (BD, #554722)
523 and stored in PBS overnight. For the extracellular and intracellular fluorescent cell staining, cells were
524 permeabilized with BD Perm/Wash buffer (BD, #554723) for 15 min. T lymphocytes were evaluated using
525 the following antibodies: rat anti-mouse IL-17A (TC11-18H10.1, 1/50; Biolegend, #506922), rat anti-mouse
526 RORγt (AFKJS-9, 1/44, eBiosciences, #17-6988-82), rat anti-mouse CD3 (17A2, 1/88, Biolegend, #100241),
527 rat anti-mouse CD45 (30-F11, 1/88, BD, #564225), rat anti-mouse CD4 (RM4-5, 1/700, Biolegend, #100548),
528 rat anti-mouse IFN-γ (XMG1.2, 1/175, eBiosciences, #61-7311-82), rat anti-mouse FOXP3 (FJK-16s, 1/200;

529 ThermoFisher, #48-5773-82), rat anti-mouse CD8 (53-6.7, 1/700, Biolegend, #100710). Optimal staining
530 concentrations of all antibodies were evaluated before staining. Cells were incubated with FACS buffer diluted
531 antibodies for 30 min at 4 °C in the dark. Samples were washed twice with 150 µL of BD Perm/Wash buffer,
532 resuspended in 200 µL PBS and acquired using Quanteon NovoCyte (NovoCyte Quanteon 4025, Agilent). All
533 acquired data were analyzed using FlowJo™ Software (version 10.7.2, BD, 2019). Fluorescence minus one
534 controls (FMOs) were used for each antibody-fluorophore combination to properly evaluate signal-positive
535 and -negative cells. Single antibody-stained UltraComp eBeads™ Compensation Beads (Fisher Scientific, Ref:
536 01-2222-42) were used to create the compensation matrix in FlowJo. Compensation samples were gated on
537 the population of compensation beads within the FSC and SSC and the positive and negative population for
538 the corresponding antibody were identified. After applying the compensation matrix, samples underwent the
539 following gating strategy: (1) identifying single live cells in a FSC-A vs. FSC-H plot; (2) selecting live cells
540 in a Zombie NIR vs. SSC plot; (3) identifying single, live $CD45^+$ cells in a $CD45^+$ vs. SSC plot. All samples
541 with less than 1000 events in this plot were removed from the analysis. FACS analysis of isolated lymphocytes
542 was performed blinded and gating strategy was verified by two persons.

543 **Illumina 16S rRNA gene sequencing and analysis**

544 Bacterial DNA extraction from colonic and ileal content was performed as described previously (*16*). A
545 Qubit® dsDNA HS assay kit was used to quantify sample inputs. The V4 region of the 16S rRNA gene was
546 amplified using dual-index primers described by Kozich et al (*54*). Library preparation was performed
547 according to manufacturer's protocol using the Quick-16S™ NGS Library Prep Kit (Zymo Research, Irvine,
548 CA, USA, #D6400). The pooled libraries were sequenced on an Illumina MiSeq using MiSeq®Reagent Kit
549 v2 (500-cycle) (Illumina, #MS_102_2003). All raw sequencing data have been uploaded to the European
550 Nucleotide Archive (ENA) at EMBL-EBI under the study accession number PRJEB60278. The program
551 mothur (v1.44.3) (*55*) was used to process the reads according to the MiSeq SOP (*54*). For gnotobiotic samples,
552 taxonomy was assigned using a k-nearest neighbor consensus approach against a custom reference database
553 corresponding to the SM14 taxa and potential contaminants (*Citrobacter rodentium*, *Lactococcus lactis* subsp.
554 *cremoris*, *Staphylococcus aureus*, and *S. epidermis*). For SPF samples, taxonomy was assigned using the Wang
555 approach against the SILVA v132 database. Count data was normalized by computing relative abundance.

556 **Construction of the phylogenetic tree of SM14 constituent strains**

557 The phylogenetic tree was constructed based on 16S rRNA gene sequences and analyzed with Geneious Prime
558 version 2021.2.2. Accession numbers of the sequences were: AY271254.1 (*A. muciniphila*), AB510697.1 (*B.*
559 *caccae*), EU136682.1 (*B. ovatus*), HQ012026.1 (*B. thetaiotaomicron*), AB050110.1 (*B. uniformis*),
560 AB370251.1 (*B. intestinihominis*), AB626630.1 (*E. rectale*), HM245954.1 (*C. symbiosum*), AJ505973.1 (*M.*
561 *formatexigens*), AF192152.1 (*D. piger*), AB011816.1 (*C. aerofaciens*), AJ413954.1 (*F. prausnitzii*),
562 AJ312385.1 (*R. intestinalis*). A neighbor-joining tree build model was created using global alignment with
563 free end and gaps, 65% similarity index cost matrix, and a Tamura-Nei genetic distance model.

564 **Metabolomics analysis of cecal contents using capillary electrophoresis-time of flight mass spectrometry**
565 **(CE-TOF/MS)**

566 Cecal metabolites were extracted from about 10 mg of a freeze-dried sample by vigorous shaking with 500 µL
567 of 100% MeOH supplemented with 20 µM methionine sulfone as well as 20 µM D-camphor-10-sulfonic acid,
568 as per internal standards. Four 3 mm zirconia beads (BioSpec Products, Bartlesville, OK, USA) and about 100
569 mg of 0.1 mm zirconia/silica beads (BioSpec Products, Bartlesville, OK, USA) were added to this mix.
570 Afterwards, samples were shaked vigorously for 5 minutes using a Shake Master NEO (BioSpec Products,
571 Bartlesville, Oklahoma, U.S.A.). Next, 500 µL of chloroform and 200 µL of Milli-Q water were added, and
572 samples were shaken vigorously for 5 minutes again and followed by centrifugation at 4600 × g for 30 min at
573 4°C. The resulting supernatant was transferred to a 5 kDa cut-off filter column (Ultrafree MC-PLHCC 250/pk)
574 for metabolome analysis (Human Metabolome Technologies, Tsuruoka, Yamagata, Japan). The flow-through
575 was dried under vacuum. Residue was dissolved in 50 µL of Milli-Q water containing reference compounds
576 (200 µM 3-aminopyrrolidine and 200 µM trimesic acid). The levels of extracted metabolites were measured
577 by CE-TOF/MS in both, positive and negative modes, using an Agilent 7100 capillary electrophoresis system
578 (Agilent Technologies, Waldbronn, Germany) equipped with an Agilent 6230 TOF LC/MS system (Agilent
579 Technologies, Santa Clara, CA, USA).

580 **Metabolite-of-interest screening pipeline**

581 Given that EAE phenotypes were disconnected from the overall metabolome pattern, we looked for single
582 metabolites which might explain observed differences in EAE disease course. Thus, we implemented a

583 screening pipeline, comprising 20 independent analyses, to identify potential metabolites-of-interest that might
584 explain differences in EAE outcomes. These analyses included evaluation of the contribution of each
585 metabolite to the variance of the PC1 and PC2 axes in a mulidimensional reduction PCA plot (**Extended Data**
586 **Fig. 3b**), correlation analyses (**Extended Data Fig. 3c**), as well as group-wise comparisons of metabolite
587 concentrations (**Extended Data Fig. 3d**). By combining information obtained from these analyses, our goal
588 was to shortlist microbiota-induced cecal metabolites that enable prediction of either the overall disease course
589 or the relapse occurrence in EAE-induced mice. We concluded that a potential metabolite-of-interest should
590 fulfill the following five criteria (1 − 5): (1) an overall significantly different concentration between all 7
591 groups (**Extended Data Fig. 3c**, "SIG"; **Extended Data Fig. 3e** "SIG"), as determined by one-way ANOVA
592 tests. As we have observed differences in EAE outcome on a group-based level, this should also be reflected
593 in different concentrations of a metabolite-of-interest between the groups. (2) a non-significant contribution to
594 the variance of the PC2 axis (**Fig. 3c**, "PC2"; **Extended Data Fig. 3b**, **Extended Data Fig. 3e** "PC2_POS",
595 "PC2_NEG"). As shown in **Fig. 3a**, different microbiota compositions were well reflected by the position of
596 individual mice on the PC1 axis. Interestingly, differences in EAE status (EAE-induced *vs.* non-EAE-induced)
597 were reflected by the position of individual mice on the PC2 axis. EAE-induced mice of all microbiota
598 compositions generally provided lower values on the PC2 axis compared to their non-EAE-induced
599 counterparts harboring the same microbiota composition. In summary, we made the following four
600 observations (i – iv): (i) Different EAE phenotypes were a consequence of different microbiota compositions;
601 (ii) Microbiota composition was well reflected by the position on the PC1 axis; (iii) EAE-induced mice of all
602 microbiota compositions provided the same shift towards lower values on the PC2 axis compared to non-EAE-
603 induced mice and (iv), as the shift towards lower values on the PC2 axis occurred in every microbiota
604 composition, we concluded that these shifts occured independent from the EAE disease phenotype given the
605 significant differences in EAE outcomes in mice harboring different microbiota compositions. In summary,
606 we concluded that these shifts on the PC2 axis were either a direct result of EAE induction (independent from
607 the disease phenotype) or a consequence of different microbiota colonization times since EAE-induced mice
608 harbored the respective microbiota for 3 more weeks compared to non-EAE-induced mice of the same
609 microbiota composition. Thus, we concluded that metabolites, which significantly contributed to the PC2 axis

610 shift, were not causal to different EAE phenotypes. Instead, their concentrations in EAE-induced mice
611 appeared to be a feedback effect from either longer colonization or EAE induction itself. In consequence, these
612 metabolites were removed from the list of metabolites-of-interest. (3) a significant correlation with either the
613 overall disease course (**Fig. 3c**, "AUC"; **Extended Data Fig. 3e**) or the mean score during the relapse phase
614 (REL) in EAE-induced mice. (4) a significant correlation with the presence of *A. muciniphila* (**Fig. 3c**, "AM",
615 **Extended Data Fig. 3e**) since we observed different EAE phenotypes based on presence or absence of *A.*
616 *muciniphila.* (5) a significantly different concentration when comparing non-EAE-induced mice harboring
617 microbiota compositions leading to different EAE phenotypes upon EAE induction (**Fig 3c, Extended Data**
618 **Fig. 3d**). This criterion would allow for assessing the prediction aspect of cecal metabolite concentrations. As
619 SM13-colonized and GF mice resulted in a moderate phenotype, SM01-colonized mice in an intermediate
620 phenotype and SM14-colonized mice in a severe phenotype, we hypothesized that a potential metabolite of
621 interest would reflect these differences by providing the following four properties (i − iv): (i) significantly
622 different concentrations when comparing "SM13 – EAE" vs "SM14 – EAE" and "SM13 + EAE" vs "SM14 +
623 EAE"; (ii) significantly different concentrations when comparing "SM13 – EAE" vs "SM01 – EAE" and
624 "SM13 + EAE" vs "SM01 + EAE"; (iii) significantly different concentrations when comparing "SM01 – EAE"
625 vs "SM14 – EAE" and "SM01 + EAE" vs "SM14 + EAE" and (iv) no significantly different concentrations
626 when comparing "SM13 – EAE" vs "GF – EAE" and "SM13 + EAE" vs "GF + EAE".

627 **Metatranscriptomics analysis**

628 Flash-frozen cecal contents were stored at –80 °C until further processing. 1 mL RNAProtect Bacterial Reagent
629 (Qiagen, #76506) was added to each sample and thawed on wet ice for 10 min. Samples were centrifuged at
630 10 000 × g, 4°C for 10 min and 250 µL acid-washed glass beads (212–300 µm), 500 µL of Buffer A (0.2 M
631 NaCl, 0.2 M Trizma base, 20 mM EDTA pH 8), 210 µL of SDS 20% and 500 µL of phenol:chloroform
632 (125:24:1) pH 4.3 were added to the pellet. Bead‐beating on the highest frequency (30 Hz) was performed
633 for 5 min using a mixer mill and the aqueous phase was recovered after centrifugation at 4°C for 3 min at 18
634 000 × g. 500 µL of phenol:chloroform (125:24:1) pH 4.3 was added to each sample and centrifuged as
635 previously described. Again, the aqueous phase was recovered and 1/10 volume of 3M sodium acetate (pH ~
636 5.5) and 1 volume of ice-cold 100% ethanol was added and gently mixed by inversion. Samples were incubated

637 for 20 min on wet ice and then washed twice with 500 µL of ice-cold 70% ethanol and centrifuged at 4°C for
638 20 min at 18 000 × g. Pellets were air-dried for 10 min and resuspended in 50 µL nuclease-free water. DNase
639 treatment was performed by adding 10 µL 10X buffer, 40 µL nuclease-free water (to reach 100 µL final
640 volume) and 2 µL DNase I (Thermo Scientific, DNase I, RNase-free kit, #EN0521) followed by 30 min
641 incubation at 37°C. 1 µL EDTA 0.5M (per sample) was added and heat-inactivated for 10 min at 65°C. RNA
642 purification was performed with the RNeasy Mini kit (QIAGEN, #74106) according to manufacturer
643 instructions. RNA quantity and a quality were assessed using the RNA 6000 Nano Kit on an Agilent 2100
644 Bioanalyzer. Library preparation was performed using an Illumina® Stranded Total RNA Prep, Ligation with
645 Ribo-Zero Plus kit (Illumina, #20040529). Pooled libraries were then run on a NextSeq 550 High Output flow
646 cell 2×75bp up to 800M reads followed by NextSeq 550 Medium Output flow cell 2x75bp up to 260M reads.
647 RNA sequencing files were pre-processed using kneaddata (https://github.com/biobakery/kneaddata).
648 Adapters were removed using Trimmomatic (16) and fragments below 50% of the total expected read length
649 (75 bp) were filtered out. BowTie2 (17) was used to map and remove contaminant reads corresponding to
650 either rRNA databases or the *Mus musculus* genome. Clean fastq files were concatenated before passing to
651 HUMAnN3 (18). A custom taxonomy table based on pooled 16S rRNA sequencing abundances was provided
652 to metaPhlan for metagenome mapping. Unaligned reads were translated for protein identification using the
653 UniRef90 database provided within HUMAnN3. Data for all samples were joined into a single table and
654 normalized using count per million (CPM) method. Results were grouped by annotated protein product per
655 individual. In case no annotation from UniRef90 transcript IDs was possible, distinct IDs were treated as
656 separate gene products. Only gene products that provided >50 CPM in at least two of the eight investigated
657 samples were included into downstream analyses. This resulted in 2213 transcripts being included into
658 downstream analyses, representing 80 % to 85 % of the total CPM with no significant differences between the
659 analyzed groups. CPM were recalculated to account for removed transcripts, followed by further analysis using
660 the *edgeR* package (version 3.38.4) in R Studio (version 4.2.1). Multidimensional reduction of the
661 transcriptome profiles was calculated using the *logFC* method within the *plotMDS.DGEList* function.
662 Groupwise comparison of gene expression was calculated using the *exactTest()* function.

663 **Bacterial IgA coating index**

664 Fecal samples stored at –20 °C were resuspended in 500 µL ice-cold sterile PBS per fecal pellet and
665 mechanically homogenized using a plastic incolulation loop. Pellets were then thoroughly shaken for 20 min
666 at 1100 rpm and 4 °C. After adding 2 × volume of ice-cold PBS, samples were centrifuged for 3 min at 100 ×
667 g and 4°C to sediment undissolved debris. Clear supernatant was recovered and passed through a 70 µm sieve
668 (Imtec, #U3_10070_70) followed by centrifugation for 5 min at 10 000 × g and 4 °C to sediment bacteria.
669 Supernatant was removed and pellet resuspended in 1 mL ice-cold PBS. Next, optical density of this
670 suspension at 600 nm (OD_{600}) was detected and approximate concentration of bacteria was estimated based on
671 the assumption that OD_{600} = 1 equals 5×10^8 bacteria per mL. The respective volume corresponding to 10^9
672 bacteria was centrifuged for 5 min at 10 000 × g and 4 °C. Pellet was then resuspended in 400 µL 5 % goat
673 serum (Gibco, #11540526) in PBS and incubated for 20 min on ice. After incubation, pellet was washed once
674 in ice-cold PBS and centrifuged for 5 min at 10 000 × g and 4 °C. Pellet was then resuspended in 100 µL ice-
675 cold PBS containing 4 µg of FITC-coupled goat anti-mouse IgA antibody (SouthernBiotech, Imtec Diagnostic,
676 #1040-02). The ratio of 4 µg of the respective antibody to stain 10^9 bacteria was previously evaluated to be the
677 maximum amount of antibody that can be used without resulting in unspecific staining of non-IgA coated
678 bacteria by using fecal samples from *Rag1*$^{-/-}$ mice as non IgA-coated negative controls. Samples were then
679 incubated for 30 min at 4 °C on a shaker at 800 rpm. After incubation, 1 mL ice-cold PBS was added followed
680 by centrifugation for 5 min at 10 000 × g and 4 °C. Samples were then washed once in ice-cold PBS, either
681 subjected for flow-cytometry detection or for separation of IgA^+ and IgA^- bacteria. For immediate flow
682 cytometric detection, pellets were resuspended in 200 µL DNA staining solution (0.9% NaCl in 0.1M HEPES,
683 pH 7.2, 1.25 µM Invitrogen SYTO™ 60 Red Fluorescent Nucleic Acid Stain, Fisher Scientific, #10194852)
684 followed by incubation for 20 min on ice. After washing once with PBS, pellets were resuspended in 100 µL
685 PBS and run immediately on a Quanteon NovoCyte (NovoCyte Quanteon 4025, Agilent). For separation of
686 IgA^+ from IgA^- negative bacteria, we used the MACS cell separation system from Miltenyi. Pellets were
687 resuspended in 100 µL staining buffer (5% goat serum in PBS) containing 10 µL anti-FITC microbeads
688 (Miltenyi, #130-048-701) per 10^9 bacteria, mixed well and incubaterd for 15 min at 4 °C. After end of
689 incubation time, 1 mL of staining buffer was added, followed by centrifugation for 5 min at 5 000 × g. Pellet
690 was then resuspended in 5 mL staining buffer per 10^9 bacteria and loaded onto MACS LD separation columns

691 (Miltenyi, #130-042-901) and flow-through containing the IgA^- fraction was collected. After removing
692 columns from the magnet, the IgA^+ fraction was flushed out and collected. The IgA^+ fraction was then loaded
693 on a MACS LS separation column (Miltenyi, #130-042-401). Flowthrough was collected and combined with
694 the previous IgA^- fraction. After removing columns from the magnet, the IgA^+ bacteria fraction was flushed
695 out, collected and combined with the previous IgA^+ fraction. Both combined fractions, IgA^+ and IgA^- were
696 then centrifuged for 10 min at 10'000 × g and 4 °C. Pellets were then resuspended in 1 mL PBS and subjected
697 to two different downstream analyses: (1) To test purity of both fractions for each sample by flow cytometry,
698 10% of the suspension volume was used for bacterial DNA staining using SYTO™ 60 Red Fluorescent Nucleic
699 Acid Stain as described above, whereas purity was generally >90% for both fractions; (2) To purify bacterial
700 DNA for subsequent 16S rRNA gene sequencing of bacteria within the different fractions, 90% of the
701 suspension volume was centrifuged for 10 min at 10 000 × g and 4 °C, supernatant was discarded and the dry
702 pellet was stored at -20 °C. DNA isolation and 16S rRNA gene sequencing was then performed as described
703 above. The IgA-coating index (*ICI*) for a given species *x* (ICI_x) was calculated by the following equation, with
704 A_x^+ representing the strain-specific relative abundance in the IgA^+ fraction and A_x^- representing the strain-
705 specific relative abundance in the IgA^- negative fraction: $ICI_x = log_{10}\left(\frac{A_x^+}{A_x^-}\right)$. Strains were classified as "highly
706 coated", when $A_x^+ > 2 \times A_x^-$ ($ICI_x > 0.301$) and as "low coated", when $ICI_x < -0.301$.

707 **Soluble IgA measurements in fecal contents**

708 We used 10 ng per well rabbit anti-mouse IgA (Novus Biologicals, #NB7506) for overnight coating of high
709 binding 384 well plates (Greiner, #781061) in 20 µl per well of carbonate-bicarbonate buffer (Sigma, #C3041).
710 Plates were then washed four times in wash buffer (10 mM Trizma Base, 154 mM NaCl, 1% (v/v) Tween-10).
711 Next, 75 µL of a blocking buffer (15 mM Trizma acetate, 136 mM NaCl, 2 mM KCl, 1% (w/v) bovine serum
712 albumin (BSA)) was added to each well and incubated for 2 h at RT. Following another washing step with was
713 buffer, samples and standards were diluted in a dilution buffer (blocking buffer + 0.1% (w/v) Tween-20). As
714 standards, we used a mouse IgA isotype control (Southern Biotech, #0106-01). 20 µL of the dilutions were
715 added to each well and incubated for 90 min at RT. Following another washing step, a secondary goat anti-
716 mouse IgA antibody, conjugated with alkaline phosphatase (Southern Biotech, # 1040-04), diluted 1:1000 in
717 dilution buffer, was added. Secondary antibody was incubated at RT for 90 min and plates were washed four

718 times. As a substrate, 1 phosphate tablet (Sigma, #S0642-200 TAB) was solubilized in 1 mM 1 mM 2-Amino-
719 2-methyle-1-propanole and 0.1 mM MgCl2.6H2O. 40 µL of this substrate solution was added to each well,
720 followed by incubation at 37 °C for 60 min. Final absorbance at 405 nm was detected using a SpectraMax Plus
721 384 Microplate Reader.

722 **Quantification of lipopolysaccharides levels in blood serum**

723 To quantify lipopolysaccharide levels in blood serum from mice, full blood was incubated for 30 min at 37
724 °C, followed by centrifugation for 30 min at 3000 × rpm and RT. Serum supernatant was then stored at −80
725 °C until use. Quantification was performed using the Pierce Chromogenic Endotoxin Quantification Kit
726 (ThermoScientific, #A39552) according to manufacturer's instructions. Thawed serum samples were heat-
727 shocked for 15 min at 70 °C and diluted 1:50 prior to performing the assay. After blank reduction, final
728 endotoxin levels were calculated based on detected optical densities (OD) of supplied standards and using
729 RStudio (version 4.2.1) using a 4-parameter nonlinear regression of standard ODs with the help of the *drc*
730 package (version 3.0.1) applying the function *drm(OD~concentration, fct=LL.4())*. Sample concentrations
731 were then extracted using the *ED(type="absolute")* function of the same package.

732 **ELISA-based quantification of zonulin and occludin concentrations in blood serum**

733 To measure concentrations of zonulin (ZO-1) and occludin (OCLN) in blood serum, we used the Mouse Tight
734 junction protein ZO-1 ELISA Kit (MyBioSource, #MBS2603798) and the Mouse Occludin (OCLN) ELISA
735 Kit (ReddotBiotech, #RD-OCLN-Mu), respectively, according to the manufacturer's instructions. After blank
736 reduction, final ZO-1 and OCLN concentrations were calculated based on detected optical densities (OD) of
737 supplied standards and using R Studio (version 4.2.1) applying a 4-parameter nonlinear regression of standard
738 ODs with the help of the *drc* package (version 3.0.1) using the function *drm(OD~concentration, fct=LL.4())*.
739 Sample concentrations were then extracted using the *ED(.., type="absolute")* function of the same package.

740 **Lipocalin-2 ELISA**

741 To measure fecal lipocalin-2 levels, the fecal pellet were homogenized in 500 µl ice-cold PBS with 1% Tween
742 20. Samples were then subjected to, agitation for 20 min at 4 °C at 2000 rpm on a thermomixer, followed by
743 centrifugation for 10 min at 21000 × g and 4 °C. Pellets were discarded, supernatants were harvested and

744 stored at –20°C until further use. Final Lipocalin-2 detection was conducted using the Mouse Lipocalin-
745 2/NGAL DuoSet Elisa, R&D Systems (# DY1857) according to the manufacturer's instructions.

746 **Detection of bacterial relative abundances using quantitative real-time PCR**

747 To detect relative abundances of commensal bacteria from fecal samples obtained from mice harboring
748 reduced communities (SM01 to SM14) in a gnotobiotic setting, we followed a protocol published elsewhere
749 (*21*) without modifications. Primer sequences for strain-specific quantification are listed in **Extended Data**
750 **Table 2**.

751 **Detection of glycan-degrading enzyme activities from mouse fecal samples**

752 To detect activities of α-fucosidase, α-galactosidase, β-glucosidase, β-*N*-acetyl-glucosaminidase and sulfatase
753 from fecal samples stored at −20 °C, we followed the protocol published in detail elsewhere (*56*) without
754 modifications.

755 **Data analysis**

756 All figures and analyses were performed using RStudio (versions 4.1.3 and 4.2.1). For details see analysis-
757 specific informations in this section.

758 **Illumina 16S rRNA gene sequencing-based analysis of complex microbial communities**

759 Groupwise analysis of annotated reads was performed using RStudio (version 4.2.1) with an initial seed set at
760 8765. All operational taxonomic units (OTUs) not constituting at least 0.1% of reads within at least one group
761 (group means) were removed from the analysis. Diversity indices were determined using the *diversity()*
762 function of the *vegan* package (version 2.6.2). Nonmetric multidimensional scaling for Bray-Curtis distance
763 matrices were calculated using the *metaMDS()* function of the *vegan* package and principal coordinate
764 decomposition of weighted UniFrac distance matrices were calculated the *pcoa()* function of the *ape* package
765 (version 5.6.2). All analyses were performed on OTU level, genus level and family level. OTUs and genera
766 contributing most to community differences between selected groups were extracted using the *simper()*
767 function of the *vegan* package.

Acknowledgements

This work was supported by the following grants in the laboratory of M.S.D.: Luxembourg National Research Fund (FNR) CORE grants (C15/BM/10318186 and C18/BM/12585940) and BRIDGES grant (22/17426243) to M. S. D; and FNR INTER Mobility grant (16/11455695) to M. S. D.; FNR AFR bilateral grant (15/11228353) support to M.N.; FNR AFR individual PhD fellowship (11602973) to A. P.; E.T.G. was supported by the FNR PRIDE grant (PRIDE17/11823097) and the Fondation du Pélican de Mie et Pierre Hippert-Faber, under the aegis of the Fondation de Luxembourg. We thank MEDICE Arzneimittel Pütter GmbH & Co. KG, Germany and Theralution GmbH, Germany for funding through the public–private partnership FNR BRIDGES grant (22/17426243). E.M. is supported by The Japan Society for the Promotion of Science (JSPS) KAKENHI (19K05907), Lotte Foundation, and Astellas Foundation for Research on Metabolic Disorders. S.F. (including CE-TOF/MS metabolomic analyses) was supported by JSPS KAKENHI (22H03541), JST ERATO (JPMJER1902), AMED-CREST (JP22gm1010009), and the Food Science Institute Foundation. We acknowledge the National Cytometry Platform (NCP) for their assistance with flow cytometry. The NCP is supported by Luxembourg's Ministry of Higher Education and Research (MESR) funding. We also thank the support of Christian Jäger, Xiangyi Dong and Floriane Gavotto from the Luxembourg Centre for Systems Biomedicine (LCSB), Metabolomics Platform for GC-MS analyses. We thank Kathy McCoy for providing us with *Muc2*$^{-/-}$ mice.

Data availability statement

The raw fastq files for this study from 16S rRNA gene sequencing and RNA sequencing have been deposited in the European Nucleotide Archive (ENA) at EMBL-EBI under accession number PRJEB60278 (https://www.ebi.ac.uk/ena/browser/view/PRJEB60278).

Conflict of interest

Author M.S.D. works as a consultant and an advisory board member at Theralution GmbH, Germany. S.F. is a founder and CEO of Metagen, Inc., Japan, focused on the design and control of the gut environment for human health.

795 # Figure legends

796 **Figure 1: Increased levels of *Akkermansia* are associated with lower neuroinflammation in EAE-induced**
797 **mice harboring a complex native microbiota.**

798 **a)** Central objective of the study: To investigate how microbiota composition interacts with the host immune
799 system (exhibits a specific "function"), influences the degree of demyelination during experimental
800 autoimmune encephalomyelitis (EAE) and results in different disease phenotypes. Microbiota composition-
801 based prediction of disease-mediating properties would make targeted microbiota manipulation
802 ("intervention") possible.

803 **b)** Experimental setting for panels c) to f). C57BL/6J mice purchased from Charles River (CR), housed under
804 SPF conditions, were fed either a fiber-rich (FR) or fiber-free (FF) diet for 20 d, followed by induction of EAE.
805 Mice were kept on the respective diets during EAE course. EAE disease development was recorded for 30 d.

806 **c)** EAE disease scores as a function of time. All mice (FR, n=20; FF, n=19; two independent experiments)
807 were scored daily at the same time. Dots represent group means; shaded area and dotted lines represent SD.
808 Statistics: daily EAE scores were compared using a Wilcoxon rank-sum test. "ns": no statistically significant
809 difference between groups at any day.

810 **d)** Area-under-the-curve (AUC) analysis of the disease course depicted in c). Each mouse depicted by a
811 separate dot. Statistics: unpaired t-test after verification of normal distribution of values using a Shapiro-Wilk
812 test. Boxplots follow standard Tukey representations.

813 **e)** Sankey diagram of key event occurrence (in % of all mice within one group) during EAE. Susceptibility:
814 score of 2.5 for at least 1 d. Remission: decrease of EAE score by 1.5 points compared to maximum score.
815 Relapse: Increase by 1.0 point compared to remission score.

816 **f)** Percentage of variance explained by diet when comparing AUC between FR and FF groups. Determined by
817 eta-squared (η^2) calculation.

818 **g)** Experimental setting for panels h) to k). *Muc2*$^{+/+}$ and *Muc2*$^{-/-}$ littermate mice were fed an FR (*Muc2*$^{+/+}$ and
819 *Muc2*$^{-/-}$) or FF (*Muc2*$^{+/+}$ only) diet for 20 d, followed by EAE induction and observation of disease course for
820 30 d. Mice were kept on their respective diets during EAE.

821 **h)** EAE disease scores as a function of time. All mice (FR-fed *Muc2*$^{+/+}$, n=5; FF-fed *Muc2*$^{+/+}$, n=5; FR-fed
822 *Muc2*$^{-/-}$, n=4) were scored daily at the same time. Dots represent group means; shaded area and dotted lines
823 represent SD. Statistics: daily EAE scores compared using a Wilcoxon rank-sum test followed by Benjamini-
824 Hochberg p-value correction for multiple comparisons. *:p<0.05. Grey asterisks: FR-fed *Muc2*$^{-/-}$ vs FR-fed
825 *Muc2*$^{+/+}$, Black asterisks: FR-fed *Muc2*$^{-/-}$ vs FF-fed *Muc2*$^{+/+}$.

826 **i)** AUC analysis of the disease course depicted in h). Each mouse depicted by a separate point. Statistics: One-
827 way ANOVA followed by Tukey's post-hoc test for groupwise comparison. ns: $p > 0.05$; ***, $p < 0.001$.

828 **j)** Sankey diagram of key event occurrence (in % of all mice within one group) during EAE. Same event
829 definitions as in e).

830 **k)** Percentage of variance explained by diet and genotype when comparing AUC between the three groups
831 depicted in h), as determined by eta-squared (η^2) calculation.

832 **l+m)** Combined analysis of microbial communities of CR mice (FF- and FR-fed), *Muc2*$^{+/+}$ mice (FF- and FR-
833 fed) and FR-fed *Muc2*$^{-/-}$ mice as determined by Illumina-based 16S rRNA gene sequencing from fecal samples
834 collected before EAE induction. All samples were analyzed together using the same analysis pipeline.

835 **l)** Genera, which in summary explained more than 70% of the variance, as calculated based on Bray-Curtis
836 dissimilarity index obtained from relative abundance data on a genus level, of fecal microbial communities
837 between WT (CR and *Muc2*$^{+/+}$, fed both diets, combined) and KO (*Muc2*$^{-/-}$) mice before EAE induction.
838 Squares: Spearman correlations between relative abundances of the selected genera before EAE induction with
839 EAE-associated readouts as calculated by pairing values within each individual mouse across all five groups.
840 Statistical significant correlations indicated by *. Barplots depict cumulative explained variance for
841 combinations of genera, ordered from bottom (highest single contribution) to top (lowest single contribution).

842 **m)** Relative abundances of the genus *Akkermansia* in fecal microbial communities before EAE induction.
843 Statistics: One-way ANOVA followed by Tukey's post-hoc test for groupwise comparison. Non-significant
844 comparisons not shown. *, $p < 0.05$; **, $p < 0.01$; ****, $p < 0.0001$.

845 **Figure 2: Removal of *Akkermansia muciniphila* from a synthetic human microbiota results in reduced**
846 **neuroinflammation in EAE-induced mice.**

847 **a)** Phylogenetic tree comprising the SM14 community (see Materials and Methods for strain designations and
848 construction of the phylogenetic tree).

849 **b)** Experimental setup. GF C57BL/6N mice were colonized with either SM14 or SM13 (SM14 w/o *A.*
850 *muciniphila*) communities. 5 d after initial colonization, mice harboring both SM combinations were either
851 switched to a fiber-free (FF) diet or were maintained on a standard chow (FR). 20 d after diet switch, EAE was
852 induced in all mice and disease course was observed for 30 d.

853 **c)** EAE disease scores as a function of time. All mice (FR-fed SM14, n=13 (three independent experients);
854 FR-fed SM13, n=11 (three independent experients); FF-fed SM14, n=10 (two independent experients); FF-fed
855 SM13, n=4) were scored daily at the same time. Left panel: FR-fed mice. Right panel: FF-fed mice. Dotted
856 lines represent SD. Statistics: daily EAE scores were compared using a Wilcoxon rank-sum test. Left panel: *
857 indicates $p < 0.05$ when comparing SM14- with SM13-colonized mice (FR-fed only). Right panel: "ns"
858 indicates $p > 0.05$ on any given day when comparing FR- (left panel) with FF-fed (right panel) mice harboring
859 the same SM combinations.

860 **d)** Sankey diagram of key event occurrence (in % of all mice within one group) during EAE. Same event
861 definition as in Fig. 1e.

862 **e)** Left panel: Area-under-the-curve (AUC) analysis of the disease course depicted in c). Each mouse depicted
863 by a separate point. Statistics: One-Way ANOVA followed by Tukey's post-hoc test. ns, $p > 0.05$; * < 0.05.
864 Right panel: Percentage of variance explained (η^2) by diet or colonization (SM combinations, "SM") when
865 comparing AUC between all 4 groups depicted in the left panel.

866 **f)** Left panel: Mean EAE score during relapse phase (day 26 to day 30). Each mouse depicted by a separate
867 point. Statistics: One-Way ANOVA followed by Tukey's post-hoc test. ns, $p > 0.05$; * < 0.05. Right panel:
868 eta-squared analysis as decribed in e).

869 **g)** Streamplots of bacterial relative abundances as a function of time (days after EAE induction). Mean relative
870 abundances per strain, group and timepoint are shown. 2-letter abbreviations of SM14- and SM13-constituent

871 strains are explained in panel a). Bacterial relative abundances were determined by 16S rRNA gene based

872 Illumina sequencing.

Figure 3: *Akkermansia muciniphila*-mediated autoimmune neuroinflammation is associated with increased cecal concentrations of γ-amino butyric acid

a–d) Identification of microbiota-induced and EAE disease course-influencing metabolites using a metabolite screening pipeline. Germ-free (GF) C57BL/6 mice were either colonized with *Akkermansia muciniphila* only (SM01), the 13SM community (SM13), the 14SM community (SM14) or remained GF. 25d after initial colonization, mice were either subjected to harvesting cecal contents ("− EAE", n = 4 per group) or were EAE-induced followed by cecal content harvest 30d after EAE induction ("+ EAE", n = 4 per group). Cecal contents were subjected to CE-TOF/MS-based metabolomics analysis. A total of 175 metabolites were identified in at least 50% of the samples in at least one group and were thus included in the overall analysis pipeline.

a) Principal component analysis (PCA) of log-normalized metabolite concentrations using a Euclidian distance matrix. Panels separated by microbiota compositions.

b) Hierachical clustering of seven groups based on scaled group means of log-normalized concentrations of each detected metabolite.

c) "Criteria intersection analysis" of the 175 detected metabolites. Criteria were categorized into "correlation criteria", summarizing the results of either statistically significant positive ("PCor") or statistically significant negative Spearman correlation ("NCor") across all samples of all groups (both, EAE-induced and non-induced mice) and "groupwise comparison criteria". Correlations referring to EAE-associated criteria ("AUC": Area under the curve of the disease course; "MAX": maximum EAE score; "SUS": susceptibility to EAE induction as defined in Fig 1c; "REL": occurrence of relapse during the last 5 days of EAE course as defined in Fig 1c) were calculated using samples of EAE-induced mice only. Groupwise comparisons include metabolites found to be significantly different between two given groups based on an unpaired t-tests of log-normalized concentrations, using a Benjamini-Hochberg (BH)-adjusted p-value (p.adjust) as significance criterion. Barplots indicate the total number of metabolites which fulfill each listed criterion. Of the total 175 metabolites, only the criteria intersections of the 18 metabolites that demonstrate a significant correlation with either AUC or REL (or both) are displayed in detail. Grey squares indicate that a given metabolite (on the y-axis) fulfilled a specific criterion (on the x-axis) while white squares indicate a failure to fulfill a given criterion.

900 **d)** Boxplots of log-normalized concentrations of γ-amino butyric acid (GABA) under EAE or non-EAE
901 induced conditions. Statistics were calculated using am unpaired t-test with BH correction for multiple
902 comparisons.

903 **e–g)** Metatranscriptomic analysis of cecal contents of non-EAE-induced SM14-colonized (n=4) and SM13-
904 colonized (n=4) mice. Analysis includes 2213 product-annotated transcripts, surpassing a threshold of 50 CPM
905 in at least 2 samples, accounting for 80–85% of the total CPM.

906 **e)** Multidimensional reduction of transcriptome profiles. In case of SM14-colonized mice, all product-
907 annotated transcripts predicted to be derived from *A. muciniphila* were removed and CPM in these samples
908 were recalculated. This allowed to compare transcriptome profiles of SM13-constituent strains in absence and
909 presence of *A. muciniphila*.

910 **f**) Volcano plot with each dot representing one transcript. Log_2-transformed ratio of fold-change (FC) relative
911 transcript abundance (Log_2FC) in SM14-colonized mice compared to SM13-colonized mice shown on the x-
912 axis. p-value of the respective log-transformed FC shown on the y-axis. Dotted line represents significance
913 threshold ($p > 0.05$). Yellow dots represent product-annotated transcripts only found in SM14-colonized mice
914 (Group CPM mean > 10). Blue dots represent product-annotated transcripts only found in SM13-colonized
915 mice. Grey dots represent product-annotated transcripts found in both groups. n represents number of product-
916 annotated transcripts.

917 **g**) Left 2 panels: Number (n) of genes and cumulative CPM (× 1000) of transcripts being expressed only in
918 either SM13-colonized or SM14-colonized mice. Right 2 panels: Number (n) of genes and cumulative CPM (
919 × 1000) of transcripts being either upregulated or downregulated in SM14-colonized mice, but present in both,
920 SM14- and SM13-colonized mice.

921 **Figure 4: Mucin-degrading capacity of the microbiota is disconnected from EAE disease course**

922 **a)** Data from 16S rRNA gene based Illumina sequencing. Relative abundances of strains, which provided
923 statistically significant differences between FR-fed SM14-colonized mice and FR-fed SM13-colonized mice,
924 as determined by one-way ANOVA followed by Tukey's post-hoc test, on the day of EAE induction ("before
925 EAE"). *, $0.01 < p < 0.05$; **, $0.001 < p < 0.01$; ***, $p < 0.001$.

926 **b)** Constituent strains of all used SM communities. Two-letter abbreviations explained in Fig. 2a.

927 **c)** EAE disease scores as a function of time. All mice (FR-fed SM03, n=5; FR-fed SM04, n=5; FR-fed SM12,
928 n=4) were scored daily at the same time. Statistics: daily EAE scores were compared using a Wilcoxon rank-
929 sum test with BH correction for multiple comparisons. Blue asterisks represent comparison with FR-fed SM13-
930 colonized mice, yellow asterisks with FR-fed SM14-colonized mice. * indicates $p < 0.05$.

931 **d)** Sankey diagram of key event occurrence (in % of all mice within one group) during EAE. Same event
932 definition as in Fig. 1e.

933 **e)** Left panel: Area-under-the-curve (AUC) analysis of the disease course depicted in c). Each mouse depicted
934 by a separate point. Middle panel: Maximum EAE score per mouse. Right panel: Mean EAE score during
935 relapse phase (d 26 to d 30). Statistics: One-way ANOVA followed by Tukey's post-hoc test. Blue font
936 indicates comparison with FR-fed SM13-colonized mice, yellow font with FR-fed SM14-colonized mice. *,
937 $0.01 < p < 0.05$; **, $p < 0.01$.

938 **Figure 5: Microbiota alterations result in three different EAE group phenotypes and two different**
939 **individual phenotypes**

940 **a)** Summary of EAE disease course of all tested colonization/diet-combinations. Heatmap summarizes data
941 from Fig. 2c, Extended Data Fig. 2 and Fig. 4c. Daily mean EAE score per colonization/diet-combination
942 visualized by color scale.

943 **b)** Summary of key EAE-associated readouts of all tested colonization/diet-combinations. Squares indicate
944 group mean. Dark grey bar indicates standard deviation (SD). SusO, occurrence of susceptibility; RemO,
945 occurrence of remission; RelM, mean EAE score during relapse phase; RelO, occurrence of disease relapse;
946 Max, maximum achieved EAE score; AUC, area-under-the-curve analysis of EAE score as a function of time.
947 For definition of "Susceptibility", "Relapse" and "Remission" see Fig. 1e.

948 **c)** Groupwise EAE phenotype classification. Cluster dendrogram of scaled group means of EAE-associated
949 readouts (panel b), based on a Euclidian distance matrix. Group phenotypes were classified according to the
950 three obtained main clusters.

951 **d)** Percentage of variance explained (η^2) by diet or SM-combinations (SM) when comparing EAE-associated
952 readouts among all colonization/diet-combinations.

953 **e)** EAE phenotype classification by mouse (individual) by applying t-stochastic neighbor embedding (t-SNE)
954 analysis to EAE-associated readouts data sets of each individual mouse across all tested colonization/diet-
955 combinations. Cluster 1 (strong EAE symptoms) and Cluster 2 (minor EAE symptoms) phenotype) resulted
956 from applying a perplexity of 20 to t-SNE analysis, using 6 initial dimensions.

957 **f)** Proportion of mice in Cluster 1 per colonization/diet-combination. Groupwise EAE phenotype classification
958 (panel c) added below.

959 **g)** Upper panel: Relative abundances of T cell subsets [%$CD45^+$], scaled by subset and organ, of those subsets
960 which provided significant differences as determined by one-way ANOVA. Lower panel: Correlations
961 between relative abundances of those subsets with key EAE-associated readouts in the same individuals. All
962 mice of all groups included irrespective of microbiota composition. Right: Hierarchical group clustering of all

963 10 tested colonization-diet combinations based on subset means of significantly different T cell subsets in the
964 spinal cords.

965 **h)** Relative abundances of T cell subsets, which were found to be statistically significant by EAE phenotype
966 cluster affiliation, as determined by unpaired t-tests. *, $0.01 < p < 0.05$; **, $p < 0.01$.

967 **Figure 6: Using IgA coating index of an inert reporter species as surrogate measure to assess EAE-**
968 **mediating properties of a given microbial community**

969 **a)** Color codes and 2-letter abbreviations of all SM14-constituent strains

970 **b)** Pearson correlation between bacterial relative abundance of each strain before EAE induction, as detected
971 by 16S rRNA gene sequencing, with several EAE-associated readouts for individual mice: AUC, area-under-
972 the-curve analysis of EAE score as a function of time; Max, maximum achieved EAE score; RelM, mean EAE
973 score during relapse phase. For AM, only SM14-colonized mice could be used for correlation analysis. For FP
974 only SM13- and SM14-colonized mice could be used. For all other strains, SM14-, SM13-, and SM12-
975 colonized mice were analysed. Mice of both dietary groups (FR and FF) were included in this analysis. Pearson
976 correlation values for association between bacterial relative abundance and AUC are shown as bar plots, for
977 Max and RelM only color-coded squares are shown. Significant correlations ($p < 0.05$) are shown in colors
978 from blue to red according to the legend; insignificant correlations are shown in dark grey only. Correlations
979 for each strain were calculated for four different microbiota (SM) combinations: SM13 only; SM14 only;
980 SM13 and SM14 combined; SM12, SM13 and SM14 combined.

981 **c)** Variance of three key EAE-associated readouts explained by relative abundance of a given strain before
982 EAE induction. Analysis performed by combining SM12-, SM13- and SM14-colonized mice irrespective of
983 fed diet.

984 **d)** Linear mixed model regression for predicted AUC with presence of the strain as an independent variable
985 and colonization as a random intercept effect.

986 **e)** Variance in IgA-coating index (ICI) explained by high-diversity background microbiota compositions
987 (SM12, SM13 and SM14) in two strains providing highest microbiota-dependencies on ICI.

988 **f)** Individual-based paired Pearson correlation of key EAE associated readouts with ICIs of SM14-constituent
989 strains before EAE induction. Mice of all colonization-diet combinations were included in this analysis. *, p
990 < 0.05 (without further distinction).

991 **g)** Correlation of *B. ovatus* ICI with AUC (left) and maximum EAE score (right) in all mice harboring *B.*
992 *ovatus*, irrespective of background microbiota.

993 **h)** Graphical summary: Taxonomic microbiota information can be used to assess the "Risk" of a given
994 individual to develop disease (as defined by a chance < 100 %). For "Predictions", as defined by a 100 %
995 chance to develop disease, host-mediated influences on the microbiota function within a given individual must
996 have to be taken into account.

997 # Extended Data Figures

998 **Extended Data Figure 1: OTU level-based microbiota analysis of SPF-housed mice**

999 16S rRNA gene-based Illumina sequencing data analyses of DNA isolated from fecal samples. All samples
1000 were analyzed together using the same analysis pipeline. Only those OTUs that provided a mean relative
1001 abundance of at least 0.01% in at least one group were included in the analyses.

1002 **a, b)** Multifactor dimensionality reduction (**a**, NMDS plot based on a Bray-Curtis distance matrix; **b**, Principal
1003 coordinate analysis (PCoA) using a weighted UniFrac distance matrix) of microbiota composition based on
1004 OTUs. Fecal samples collected the day before EAE induction. **a**) Left panel shows clustering of samples by
1005 group, middle and right panel depict the same samples on the same two-dimensional scale as the left panel,
1006 colored by susceptibility to EAE or occurrence of relapse in the same mouse from which the respective sample
1007 was obtained. Ellipses represent 95% confidence interval for each group. The minor differences between
1008 groups in b), compared to more prominent differences between groups in a) indicate that the detected
1009 differences in the NMDS plot (a) are mostly based on phylogenetically related OTUs.

1010 **c, d)** Multifactor dimensionality reduction (c, NMDS plot based on a Bray-Curtis distance matrix; d, Principal
1011 coordinate analysis (PCoA) using a weighted UniFrac distance matrix) of microbiota composition based on
1012 OTUs. Fecal samples were collected at day 10 to 18 ("MID") or at day 30 ("END") after EAE induction.
1013 Ellipses represent 95% confidence interval for each group. Detected shifts during EAE disease course using
1014 both methods of multifactor dimensionality reduction were disconnected from group EAE phenotype (**Fig. 1**).

1015 **e)** Alpha-diversity analysis of microbiota composition before and during EAE, separated by groups and
1016 diversity indices. Fecal samples collected the day before EAE induction ("START"), at day 10 to 18 ("MID")
1017 or at day 30 ("END") after EAE induction. Observations = number of detected taxa (OTUs). Statistics:
1018 statistical differences were calculated by One-way ANOVA per panel, followed by a Tukey's post-hoc test for
1019 groupwise comparison. Statistical differences between groups before EAE induction (START) are indicated
1020 by a compact letter display; two groups sharing an assigned letter, $p > 0.05$; two groups not sharing an assigned
1021 letter, $p < 0.05$ (without further distinction). Statistical differences between different timepoints within the
1022 same groups are indicated by asterisks: *, $p < 0.05$; **, $p < 0.01$; ***, $p < 0.001$; ****, $p < 0.0001$. Non-
1023 significant comparisons are not shown.

1024 **f)** Intersection analysis to identify taxa, which are either present or absent only in *Muc2*$^{-/-}$ mice. Taxa were
1025 considered "present" within a certain group, when group mean relative abundance of a given taxon was >
1026 0.01%. Otherwise, taxa were considered "absent" in the respective group. Left panels: intersection sizes of
1027 OTUs between the five groups. Three different intersection sizes are shown ("Distinct", "Intersect", and
1028 "Union"), which are explained in the lower panels. Middle panel: Venn diagram highlighting the number of
1029 shared and distinct OTUs between the groups. Dark red, taxa only present in *Muc2*$^{-/-}$ mice; teal, taxa not
1030 present in *Muc2*$^{-/-}$ mice, but in all other mice; orange, core microbiome shared by mice of all five groups. List
1031 of OTUs belonging to these three groups provided on the right.

1032 **Extended Data Figure 2: EAE disease course in germ-free as well as SM01-, SM13- and SM14-colonized**
1033 **mice**

1034 **a)** Left panel: maximum achieved EAE score per individual within FR-fed SM13-colonized mice (n=11), FF-
1035 fed SM13-colonized mice (n=4), FR-fed SM14-colonized mice (n=13) and FF-fed SM14-colonized mice
1036 (n=10). Each mouse depicted by a separate dot in the boxplot. Statistics: One-way ANOVA followed by
1037 Tukey's post-hoc test. No statistically significant group differences observed. Right panel: Percentage of
1038 variance explained by diet ("diet", FR vs. FF) and SM combination ("SM", SM13 vs. SM14) as determined
1039 by eta-squared (η^2) calculation when comparing the maximum achieved EAE score during the 30 d disease
1040 observation period between FR- and FF-fed SM14- and SM13-colonized mice.

1041 **b–d)** GF C57BL/6 mice were either monocolonized with *A. muciniphila* (SM01) or remained germ free (GF).
1042 GF mice were fed either FR or FF diet. SM01 mice were only fed FR diet. EAE was induced in GF mice 20 d
1043 after diet switch. EAE was induced in SM01-colonized mice 25 d after initial colonization. Disease course in
1044 all groups was observed for 30 days after EAE induction.

1045 **b)** EAE disease scores as a function of time (days after EAE induction) for FR-fed GF mice (n=4), FF-fed GF
1046 mice (n=4) and FR-fed SM01-colonized mice (n=5). Dots represent daily group means. Dotted lines represent
1047 SD.

1048 **c)** Sankey diagram of key event occurrence (in % of all mice within one group) during EAE. Same event
1049 definition as in Fig. 1e.

1050 **d)** Area-under-the-curve (AUC) analysis of the disease course depicted in b). Each mouse depicted by a
1051 separate point. Statistics: One-way ANOVA followed by Tukey's post-hoc test. No statistically significant
1052 group differences observed.

1053 **Extended Data Figure 3: Metabolite-of-interest analysis pipeline**

1054 **a)** Principal component analysis (PCA) of log-normalized metabolite concentrations using a Euclidian distance
1055 matrix. Each dot represents an individual EAE-induced mouse, independent of microbiota composition. Dot
1056 colors represent EAE severity in each individual mouse (n=16), with strong EAE phenotypes colored in red.
1057 Severity represented by either AUC values of the individual EAE disease course as a function of time (left
1058 panel) or the mean score during the relapse phase ("RelM"; right panel). EAE phenotypes were disconnected
1059 from the overall metabolome pattern.

1060 **b)** Biplot showing the loadings of each metabolite, indicating significant positive or negative contribution to
1061 the PC1 and PC2 axes of a principal component analysis (PCA) of log-normalized metabolite concentrations
1062 using a Euclidian distance matrix (panel a, Fig. 3a). Each metabolite represented by one dot. Metabolites were
1063 classified as having a significant contribution when their loadings were either smaller than −0.09 or higher
1064 than +0.09 for both, PC1 (white circles with red lines) and PC2 (red circles). The total number of metabolites
1065 with significant contributions is shown on the top (for PC1) or the right (for PC2).

1066 **c)** Pearson's correlation of metabolite concentrations with key EAE-associated readouts: "Sus" = Occurrence
1067 of susceptibility (categorical); "RelM" = Mean EAE disease score during relapse phase (numerical); "Max" =
1068 maximum achieved EAE score (numerical); "AUC" = Area-under-the-curve analysis of daily EAE scores as
1069 a function of time (numerical). Only samples from EAE-induced mice were used for analysis. Significant
1070 correlations are shown in either blue (positive) or red (negative). Non-significant correlations were removed
1071 from the figure. Metabolites are listed under their KEGG-ID. A list of metabolite names with corresponding
1072 KEGG-IDs is provided in Extended Data Table 3.

1073 **d)** Volcano plot of groupwise comparison for metabolite concentrations between the groups as indicated by
1074 the color-coded legend. Each dot represents one metabolite. Significantly different expressed metabolites are
1075 highlighted in red. Benjamini-Hochberg correction was used to adjust p-values.

1076 **e)** Criteria intersection analysis of all 175 detected metabolites. Metabolites are listed under their KEGG-ID.
1077 Fulfilled criteria indicated by a dark grey square; not fulfilled criteria indicated by a white square. Criteria
1078 were categorized into "correlation criteria", summarizing the results of either statistically significant positive
1079 ("PCor") or statistically significant negative Spearman correlation ("NCor") across all samples of all groups

1080 (both, EAE-induced and non-induced mice) and "groupwise comparison criteria". Correlations referring to
1081 EAE-associated criteria ("AUC", Area under the curve of the disease course; "MAX", maximum EAE score;
1082 "SUS", susceptibility to EAE induction as defined in Fig 1c; "REL", occurrence of relapse during the last 5
1083 days of EAE course as defined in Fig 1e) were calculated using samples of EAE-induced mice only. Groupwise
1084 comparisons include metabolites found to be significantly different between two given groups based on an
1085 unpaired t-tests of log-normalized concentrations, using a BH-adjusted p-value (p.adjust) as the significance
1086 criterion (p.adjust < 0.05).

1087 **Extended Data Figure 4: Analysis of barrier integrity and mucin-associated glycan degrading capacities**
1088 **of reduced microbiota compositions**

1089 **a)** Colonization verification. Relative abundance of bacterial strains in SM03-, SM04- and SM12-colonized
1090 mice after initial colonization as detected by qPCR using strain-specific primers (Extended Data Table 2).

1091 **b–g)** Given that two of the three SM combinations which resulted in a "severe" phenotype (Fig. 4c, Fig. 5c)
1092 comprised the full set of mucin glycan-degrading strains (*A. muciniphila, B. caccae, B. instinihominis, B.*
1093 *thetaiotaomicron*) within the SM14 community and given that increased activities of microbial mucin-glycan
1094 degrading enzymes, as detected from fecal samples, were previously reported to be associated with increased
1095 susceptiblity towards enteropathogenic infections (*16*), we detected activities of *N*-acetylglucosaminidase
1096 (Nag), α-fucosidase (Fuc) and sulfatase (Sulf) (*56*), which are involved in degradation of mucin-associated
1097 glycan structures (*16*). As controls, we also detected activities of enzymes involved in fermentation of mostly
1098 plant-derived fiber structures: α-glucosidase (Gluc) and β-galactosidase (Gal). Enzyme activities were
1099 measured at three different timepoints ("periods") during the 30 d of EAE disease course: Before EAE
1100 induction ("START"), during the phase with the maximum EAE score ("PEAK") which corresponded to day
1101 14 to day 20, dependent on the individual, as well as during the remission phase ("REM") which corresponded
1102 to day 21 to day 25 after EAE induction.

1103 **b)** Left panel: Boxplot of enzyme activities of Fuc, Gal, Gluc, Nag and Sulf as determined from fecal samples
1104 collected before EAE induction (START). Each dot represents one individual mouse. Statistics: statistical
1105 differences were calculated by One-way ANOVA per enzyme, followed by a Tukey's post-hoc test for
1106 groupwise comparison. Statistical differences between groups before EAE induction (START) are indicated
1107 by a compact letter display: two groups sharing an assigned letter, $p > 0.05$; two groups not sharing an assigned
1108 letter, $p < 0.05$ (without further distinction). Right panel: Changes of enzyme activities per group during EAE
1109 disease course from START over PEAK to REM. Dots represent group means, vertical lines SD. Not all groups
1110 groups were detected at PEAK or REM.

1111 **c)** Boxplot of enzyme activities of Fuc, Gal, Gluc, Nag and Sulf as determined from fecal samples in EAE-
1112 induced mice, based on cluster affiliation and period after EAE induction. Same period definition as above;

1113 same cluster definition as in Fig. 5e. Each dot represents one individual mouse. Statistics: student's t-test. *, p
1114 < 0.05; ns, non significant.

1115 **d)** Variance in enzymatic activities Fuc, Nag, Sulf, Gluc and Gal explained by microbiota composition ("SM"),
1116 diet ("Diet") or period ("Period"; START vs. PEAK vs. REM) as determined by eta-squared (η^2) calculation.
1117 While the microbiota composition turned out to be most determining factor for the different enzyme activities,
1118 diet only explained a considerable proportion of the variance for the two plant glycan-derived fiber-degrading
1119 enzymes Gluc and Gal. The timepoint of sampling during EAE course explained between 9% and 16% of the
1120 variances, suggesting that enzyme activities are, at least in part, either impacted by the current state of
1121 neuroinflammation or involved in mediating the current state of neuroinflammation

1122 **e)** Pearson's correlation coefficients of fecal enzymatic activities of Fuc, Nag, Sulf, Gluc and Gal in EAE-
1123 induced mice with EAE scores at the same day of fecal sampling for each individual. Upper panel: all mice of
1124 all microbiota–diet combinations combined ("All groups"). Lower panel: only those mice were included in
1125 correlation analyses that belonged to the respective colonization–diet combinations. Statistically significant
1126 correlations ($p < 0.05$) are marked with * without further distinction. Only Nag activities correlated
1127 significantly with EAE scores at the same day when considering all mice independent from the microbiota
1128 composition. We observed considerable differences when including only mice harboring the same microbiota
1129 composition, or the same diet or both, into such analyses (lower panel), highlighting that enzyme activity-EAE
1130 readout correlations strongly depended on the microbiota composition.

1131 **f)** Pearson's coefficients of correlations of enzymatic activities Fuc, Nag, Sulf, Gluc and Gal in fecal samples
1132 of EAE-induced mice before EAE induction with key EAE-associated readouts after EAE-induction in the
1133 same individuals. SusO, occurrence of susceptibility; RemO, occurrence of remission; RelM, mean EAE score
1134 during relapse phase; RelO, occurrence of disease relapse; Max, maximum achieved EAE score; AUC, area-
1135 under-the-curve analysis of EAE score as a function of time. All mice of all groups combined. No statistically
1136 significant correlations were determined. Consequently, no enzyme activity before EAE induction could
1137 predict any of the six key EAE-associated readouts when combining all mice of all colonization–diet
1138 combinations.

1139 **g)** Pearson's coefficients of correlations of enzyme activities during PEAK with EAE scores during remission
1140 phase ("RemS") of the same indiviual. Mice from all microbiota–diet combinations combined. Only Nag
1141 activites during the Peak phase could be used to predict EAE scores during the remission phase. Nag activities
1142 correlated positively with higher EAE scores, or in other words, less remission. This correlation was
1143 significant, but relatively weak.

1144 **h–j)** Given the significant correlation of Nag activities with certain EAE-associated readouts, we next
1145 addressed whether increased Nag activities might contribute to decreased mucosal barrier integrity and
1146 whether this might impact EAE development. It has previously been shown that increased Nag activities were
1147 associated with impairment of the intestinal mucus layer and increased lipocalin secretion into the intestinal
1148 lumen (*16*). Furthermore, reduced mucosal barrier integrity is discussed as a contributing factor to MS
1149 pathology (*57, 58*). Since we did not assess mucus layer thickness directly, we detected indirect measures of
1150 mucosal barrier integrity, such as serum levels of lipopolysaccharides (LPS), occludin and zonulin, as well as
1151 lipocalin concentrations from fecal samples. Additionally, we assessed short-chain fatty acid (SCFAs)
1152 concentrations given their contribution to maintenance of mucosal barrier integrity (*59, 60*) and the disease-
1153 alleviating properties of propionate in MS patients (*4*) and EAE-induced mice (*61*).

1154 **h)** Fecal concentrations of lipocalin (LCN) and serum concentrations of lipopolysaccharide (LPS), occludin
1155 (OCCL) and zonulin (ZO-1) as determined either from non-EAE-induced mice (−EAE) or in EAE-induced
1156 mice, 30 d after EAE-induction (+EAE). Some group/readout/timepoint combinations were not determined.
1157 Statistics: Statistical differences were calculated by One-way ANOVA per panel. ns, no statistically significant
1158 differences.

1159 **i)** Pearson's coefficients of correlations between fecal LCN concentrations, serum OCCL concentrations,
1160 serum LPS concentrations and serum LCN concentrations before induction of EAE with key EAE-associated
1161 readouts in the same individual across all tested microbiota–diet combinations. SusO, occurrence of
1162 susceptibility; RemO, occurrence of remission; RelM, mean EAE score during relapse phase; RelO,
1163 occurrence of disease relapse; Max, maximum achieved EAE score; AUC, area-under-the-curve analysis of
1164 EAE score as a function of time. No statistically significant correlations could be determined.

1165 **j)** Fecal concentrations of short-chain fatty acids (SCFA) in non-EAE-induced mice of certain microbiota–diet
1166 combinations. Statistics: statistical differences were calculated by One-way ANOVA per SCFA, followed by
1167 a Tukey's post-hoc test for groupwise comparison. Statistical differences between groups are indicated by a
1168 compact letter display: two groups sharing an assigned letter, $p > 0.05$; two groups not sharing an assigned
1169 letter, $p < 0.05$ (without further distinction). SCFA concentrations were unrelated to EAE disease phenotypes
1170 upon EAE induction.

1171 **Extended Data Figure 5: T cell polarisation in EAE-induced and non-EAE-induced mice**

1172 **a)** Boxplots of relative abundances of certain T cell populations in various organs. Group means of these
1173 populations are summarized in the heatmap shown in Fig. 5g. Colon, ileum, mesenteric lymphnodes and spinal
1174 cords were harvested followed by isolation of lymphocytes. Isolated lymphocates were subjected to flow
1175 cytometry-based analyses and relative abundances of subpopulations were calculated as percentage of CD45-
1176 expressing cells. LP, lamina propria. Each dot represents one individual. Groups are arranged based on their
1177 EAE group phenotype classification (Fig. 5c). Severe phenotype on the left: FR-fed SM04 ("SM04 FR"), FR-
1178 fed SM03 ("SM03 FR"), FR-fed SM14 ("SM14 FR"). Intermediate phenotype in the middle: FR-fed SM01
1179 ("SM01 FR"), FF-fed SM14 ("SM14 FF"). Moderate phenotype on the right: FF-fed germ-free mice ("GF
1180 FF"), FF-fed SM13 ("SM13 FF"), FR-fed SM13 ("SM13 FR"), FR-fed germ-free ("GF FR"), FR-fed SM12
1181 ("SM12 FRF"). Statistics: only population-organ combinations with statistically significant differences, as
1182 calculated by One-way ANOVA, are shown. Tukey's honestly significant difference tests (Tukey HSD) were
1183 applied to subsequently determine statistically different value distribution between all groups within each
1184 population-organ combination. Statistical differences are indicated by a compact letter display. Two groups
1185 sharing an assigned letter, $p > 0.05$. Two groups not sharing an assigned letter, $p < 0.05$ (without further
1186 distinction).

1187 **b–d)** Analysis of T cell populations in non EAE-induced mice. Same populations were analyzed as shown in
1188 panel a. Only SM14-, SM13-, SM04-, SM03 and SM01-colonized mice were analyzed. All mice remained on
1189 a FR diet. Mice were analzyed after 25 days of colonization, representing the timepoint of EAE induction in
1190 EAE-induced mice. Colon, ileum, mesenteric lymphnodes and spinal cords were harvested followed by
1191 isolation of lymphocytes. Isolated lymphocytes were subjected to FACS-based analysis using the same
1192 antibody panels as used for EAE-induced mice.

1193 **b)** Boxplots of relative abundances of certain T cell populations in various organs. Each dot represents one
1194 invidual. Groups are arranged based on their EAE group phenotype classification (Fig. 5c). Statistics: only
1195 population-organ combinations with statistically significant differences are shown, as calculated by One-way
1196 ANOVA. Tukey's honestly significant difference tests (Tukey HSD) were applied to subsequently determine
1197 statistically different value distribution between all groups within each population-organ combination.

1198 Statistical differences are indicated by a compact letter display. Two groups sharing an assigned letter, $p >$
1199 0.05. Two groups not sharing an assigned letter, $p < 0.05$ (without further distinction).

1200 **c)** Pearson correlation matrix between group means of certain T cell subsets (vertical) isolated from different
1201 organs of non-EAE-induced mice with group means of EAE-associated readouts of EAE-induced mice
1202 harboring the same microbiota compositions (SM combinations, irrespective of the diet) as the non-EAE-
1203 induced mice. Non-significant correlations not shown. We found $CD4^{+}IL\text{-}17^{+}$ and $CD4^{+}IL\text{-}17^{+}IFN\gamma^{+}$ cell
1204 populations in the colonic LP, spinal cords and the ileal LP to correlate significantly. This indicated that the
1205 microbiota composition already primed $CD4^{+}$ T cells into a pro-inflammatory Th17 response before EAE-
1206 induction.

1207 **d)** Hierarchical group clustering of all 5 tested SM combinations based on scaled group means of significantly
1208 different T cells subsets, as determined by one-way ANOVA, separated by organ. Color codes indicate
1209 corresponding EAE group phenotype in EAE-induced mice, as determined in Fig. 5c. Population distribution
1210 in the colon that aligned best with emerging EAE group phenotypes upon EAE induction, indicating a crucial
1211 contribution of T cell priming in the colon by the microbiota to EAE disease course.

1212 **e)** Gating strategy to identify T cell subsets from colonic LP, MLN, SI and SC. Depicted is an example of a
1213 colonic LP-derived sample from a EAE-induced SM14-colonized mouse. Antibody-conjugated fluorochromes
1214 are indicated on the axis labels. Detection channels indicated in brackets. Black lines and squares indicate
1215 gates.

1216 **Extended Data Figure 6: Microbiota-associated predictors for EAE development**

1217 **a)** Bacterial relative abundances of SM12-, SM13- and SM14-colonized mice, as detected by 16S rRNA gene
1218 sequencing, before induction of EAE. No distinction between diets.

1219 **b)** Linear mixed model regression for predicted maximum score during EAE (Max) and mean score during
1220 relapse phase (RelM) with presence of the strain as an independent variable and colonization as a random
1221 intercept effect.

1222 **c)** Concentrations of secretory IgA, determined from fecal samples and normalized to fecal weights. Fecal
1223 samples collected 30 d after EAE induction. Each dot represents one individual mouse. Mice grouped by
1224 individual EAE phenotype, as determined in **Fig. 5e**. Cluster 1, strong EAE symptoms; Cluster 2, mild EAE
1225 symptoms. Statistics: Wilcoxon rank-sum test. Intestinal secretory IgA levels after 30 d of EAE were
1226 independent ($p = 0.271$) from the respective individual EAE phenotype clusters.

1227 **d)** Concentrations of secretory IgA, determined from fecal samples and normalized to fecal weights. Fecal
1228 samples collected 30 d after EAE induction. Each dot represents one individual mouse. Mice grouped by
1229 colonization–diet combination and EAE induction status. "- EAE": non-EAE-induced mice. "+ EAE": EAE-
1230 induced mice. Statistics: Kruskal-Wallis test followed by Wilcoxon rank-sum test for groupwise comparisons.
1231 Statistical differences are indicated by a compact letter display. Two groups sharing an assigned letter, $p >$
1232 0.05. Two groups not sharing an assigned letter, $p < 0.05$ (without further distinction). IgA levels after 30 d of
1233 EAE were significantly higher in mice harboring SM combinations with 12 or more strains. Right panel:
1234 variance of secretory IgA concentrations explained by either colonization (SM) or diet (Diet).

1235 **e)** Correlation between susceptibility (see **Fig. 1e** for definition) incidence in EAE-induced mice harboring a
1236 certain SM combination with mean secretory IgA levels in fecal samples obtained from non-EAE-induced
1237 mice harboring the same SM combination. Each dot represents one SM combination. Soluble IgA amounts, as
1238 detected from fecal samples, were a good predictor for susceptibility to disease upon EAE induction on a group
1239 level.

1240 **f)** IgA-coating index (ICI) of each strain dependent on SM combination. Each dot represents a sample obtained
1241 from one individual mouse. Statistics: One-way ANOVA. *, $p < 0.05$; ns, non significant.

1242 **g)** Variance in IgA-coating index (ICI) explained by background microbiota compositions (SM12, SM13 and
1243 SM14)

1244 **h)** Classification of SM14-constituent strains as IgA high-coated, low-coated or intermediate, dependend on
1245 microbiota composition. High coated, ICI > log(2); low coated, ICI < log(0.5); intermediate, log(0.5) < ICI <
1246 log(2).

1247 **Extended Data Figure 7: Graphical summary of experiments, analyses and conclusion**

1248 Based on the observation that low relative abundance of *Akkermansia muciniphila* (yellow rod-shape) in
1249 complex microbiota-harboring mice was associated with severe EAE development (red circle), and higher
1250 abundances of this species was associated with moderate disease (green circle) (OBSERVATION 1), we
1251 wondered whether either presence or the relative abundance of *A. muciniphila* before induction of EAE could
1252 predict subsequent disease development (QUESTION). To do so, we induced EAE in mice harboring 6
1253 different combinations of a well-characterised 14-strain consortium under gnotobiotic conditions (TEST
1254 CAUSALITY). In mice harboring these microbiotas, *A. muciniphila* was either present or absent, and if
1255 present, *A. muciniphila* provided either high or low relative abundances. We found that distinct microbiota
1256 compositions resulted in "high risk" and "low risk" microbiota compositions, as determined by the proportion
1257 of mice developing severe disease (OBSERVATION 2). Given the fact that a certain microbiota composition
1258 did not result in equal disease susceptibility in every mouse harboring this particular microbiota, we aimed at
1259 identifying potential individual microbiota-associated disease predictors (IDENTIFICATION OF
1260 INDIVIDUAL MICROBIOTA-ASSOCIATED DISEASE PREDICTORS). We found that neither relative
1261 abundance, nor the presence or absence of *A. muciniphila*, or any other strain of the tested consortium, could
1262 reliably predict EAE development across distinct communities in individual mice. However, we identified the
1263 pre-EAE IgA coating index of another consortium member strain, *B. ovatus*, to significantly correlate with
1264 individual EAE outcome after disease induction, irrespective of the microbiota composition. Thus, we
1265 conclude that making predictions on EAE development based on microbiota characteristics (or in other words,
1266 assessing the individual disease risk) is possible. However, it needs to take into account inter-microbial
1267 interactions ("networks") within a given, individual community as well as host-specific responses to a certain
1268 microbiota composition (CONCLUSION).

1269

1270 **Extended Data Figure 8: EAE scoring scheme**

1271 This decision tree depicts how daily assesment of EAE scores was performed. Blue boxes indicate instructions
1272 on mouse handling and EAE phenotype-associated questions (Q). Red boxes indicate possible answers (A) to
1273 the questions (Q). Green circles indicate the resulting EAE score. All arrows (answer options) are mutually
1274 exclusive.

1275 **References:**

1276 1. E. Miyauchi, C. Shimokawa, A. Steimle, M. S. Desai, H. Ohno, The impact of the gut microbiome on
1277 extra-intestinal autoimmune diseases. *Nat Rev Immunol* **23**, 9-23 (2022).
1278 2. K. Berer *et al.*, Gut microbiota from multiple sclerosis patients enables spontaneous autoimmune
1279 encephalomyelitis in mice. *Proc Natl Acad Sci U S A* **114**, 10719-10724 (2017).
1280 3. S. Miyake *et al.*, Dysbiosis in the Gut Microbiota of Patients with Multiple Sclerosis, with a Striking
1281 Depletion of Species Belonging to Clostridia XIVa and IV Clusters. *PLoS One* **10**, e0137429 (2015).
1282 4. A. Duscha *et al.*, Propionic Acid Shapes the Multiple Sclerosis Disease Course by an
1283 Immunomodulatory Mechanism. *Cell* **180**, 1067-1080 e1016 (2020).
1284 5. S. Jangi *et al.*, Alterations of the human gut microbiome in multiple sclerosis. *Nat Commun* **7**, 12015
1285 (2016).
1286 6. I. Cosorich *et al.*, High frequency of intestinal TH17 cells correlates with microbiota alterations and
1287 disease activity in multiple sclerosis. *Sci Adv* **3**, e1700492 (2017).
1288 7. E. Cekanaviciute *et al.*, Gut bacteria from multiple sclerosis patients modulate human T cells and
1289 exacerbate symptoms in mouse models. *Proc Natl Acad Sci U S A* **114**, 10713-10718 (2017).
1290 8. R. E. Ventura *et al.*, Gut microbiome of treatment-naive MS patients of different ethnicities early in
1291 disease course. *Sci Rep* **9**, 16396 (2019).
1292 9. D. Takewaki *et al.*, Alterations of the gut ecological and functional microenvironment in different
1293 stages of multiple sclerosis. *Proc Natl Acad Sci U S A* **117**, 22402-22412 (2020).
1294 10. M. C. E. a. s. b. u. e. i, M. C. i, Gut microbiome of multiple sclerosis patients and paired household
1295 healthy controls reveal associations with disease risk and course. *Cell* **185**, 3467-3486 e3416 (2022).
1296 11. E. Miyauchi *et al.*, Gut microorganisms act together to exacerbate inflammation in spinal cords. *Nature*
1297 **585**, 102-106 (2020).
1298 12. J. Ochoa-Reparaz *et al.*, A polysaccharide from the human commensal Bacteroides fragilis protects
1299 against CNS demyelinating disease. *Mucosal Immunol* **3**, 487-495 (2010).
1300 13. A. Mangalam *et al.*, Human Gut-Derived Commensal Bacteria Suppress CNS Inflammatory and
1301 Demyelinating Disease. *Cell Rep* **20**, 1269-1277 (2017).
1302 14. E. Cekanaviciute *et al.*, Multiple Sclerosis-Associated Changes in the Composition and Immune
1303 Functions of Spore-Forming Bacteria. *mSystems* **3**, (2018).
1304 15. N. Wilck *et al.*, Salt-responsive gut commensal modulates T(H)17 axis and disease. *Nature* **551**, 585-
1305 589 (2017).
1306 16. M. S. Desai *et al.*, A Dietary Fiber-Deprived Gut Microbiota Degrades the Colonic Mucus Barrier and
1307 Enhances Pathogen Susceptibility. *Cell* **167**, 1339-1353 e1321 (2016).
1308 17. M. Neumann *et al.*, Deprivation of dietary fiber in specific-pathogen-free mice promotes susceptibility
1309 to the intestinal mucosal pathogen Citrobacter rodentium. *Gut Microbes* **13**, 1966263 (2021).
1310 18. M. Van der Sluis *et al.*, Muc2-deficient mice spontaneously develop colitis, indicating that MUC2 is
1311 critical for colonic protection. *Gastroenterology* **131**, 117-129 (2006).
1312 19. E. C. Martens, M. Neumann, M. S. Desai, Interactions of commensal and pathogenic microorganisms
1313 with the intestinal mucosal barrier. *Nat Rev Microbiol* **16**, 457-470 (2018).
1314 20. S. Liu *et al.*, Oral Administration of miR-30d from Feces of MS Patients Suppresses MS-like
1315 Symptoms in Mice by Expanding Akkermansia muciniphila. *Cell Host Microbe* **26**, 779-794 e778
1316 (2019).
1317 21. A. Steimle *et al.*, Constructing a gnotobiotic mouse model with a synthetic human gut microbiome to
1318 study host–microbe cross talk. *STAR Protocols* **2**, (2021).
1319 22. J. Singh *et al.*, Urinary and Plasma Metabolomics Identify the Distinct Metabolic Profile of Disease
1320 State in Chronic Mouse Model of Multiple Sclerosis. *J Neuroimmune Pharmacol* **14**, 241-250 (2019).
1321 23. L. M. Poisson *et al.*, Untargeted Plasma Metabolomics Identifies Endogenous Metabolite with Drug-
1322 like Properties in Chronic Animal Model of Multiple Sclerosis. *J Biol Chem* **290**, 30697-30712 (2015).
1323 24. D. M. Johanson, 2nd *et al.*, Experimental autoimmune encephalomyelitis is associated with changes
1324 of the microbiota composition in the gastrointestinal tract. *Sci Rep* **10**, 15183 (2020).
1325 25. Y. Rao *et al.*, Gut Akkermansia muciniphila ameliorates metabolic dysfunction-associated fatty liver
1326 disease by regulating the metabolism of L-aspartate via gut-liver axis. *Gut Microbes* **13**, 1-19 (2021).
1327 26. M. Lopez-Siles, S. H. Duncan, L. J. Garcia-Gil, M. Martinez-Medina, Faecalibacterium prausnitzii:
1328 from microbiology to diagnostics and prognostics. *ISME J* **11**, 841-852 (2017).

1329 27. N. Feizi *et al.*, CD8(+) T cells specific for cryptic apoptosis-associated epitopes exacerbate
1330 experimental autoimmune encephalomyelitis. *Cell Death Dis* **12**, 1026 (2021).
1331 28. O. L. Rojas *et al.*, Recirculating Intestinal IgA-Producing Cells Regulate Neuroinflammation via IL-
1332 10. *Cell* **176**, 610-624 e618 (2019).
1333 29. A. Mathias, B. Pais, L. Favre, J. Benyacoub, B. Corthesy, Role of secretory IgA in the mucosal sensing
1334 of commensal bacteria. *Gut Microbes* **5**, 688-695 (2014).
1335 30. A. Pu, D. S. W. Lee, B. Isho, I. Naouar, J. L. Gommerman, The Impact of IgA and the Microbiota on
1336 CNS Disease. *Front Immunol* **12**, 742173 (2021).
1337 31. A. K. Probstel *et al.*, Gut microbiota-specific IgA(+) B cells traffic to the CNS in active multiple
1338 sclerosis. *Sci Immunol* **5**, (2020).
1339 32. N. W. Palm *et al.*, Immunoglobulin A coating identifies colitogenic bacteria in inflammatory bowel
1340 disease. *Cell* **158**, 1000-1010 (2014).
1341 33. S. K. Tankou *et al.*, Investigation of probiotics in multiple sclerosis. *Mult Scler* **24**, 58-63 (2018).
1342 34. M. Wolter *et al.*, Leveraging diet to engineer the gut microbiome. *Nat Rev Gastroenterol Hepatol* **18**,
1343 885-902 (2021).
1344 35. K. Rawat, N. Singh, P. Kumari, L. Saha, A review on preventive role of ketogenic diet (KD) in CNS
1345 disorders from the gut microbiota perspective. *Rev Neurosci* **32**, 143-157 (2021).
1346 36. K. F. Al *et al.*, Fecal microbiota transplantation is safe and tolerable in patients with multiple sclerosis:
1347 A pilot randomized controlled trial. *Mult Scler J Exp Transl Clin* **8**, 20552173221086662 (2022).
1348 37. S. N. Choileain *et al.*, CXCR3+ T cells in multiple sclerosis correlate with reduced diversity of the gut
1349 microbiome. *J Transl Autoimmun* **3**, 100032 (2020).
1350 38. T. M. Greiling *et al.*, Commensal orthologs of the human autoantigen Ro60 as triggers of
1351 autoimmunity in lupus. *Sci Transl Med* **10**, (2018).
1352 39. P. Bianchimano *et al.*, Mining the microbiota to identify gut commensals modulating
1353 neuroinflammation in a mouse model of multiple sclerosis. *Microbiome* **10**, 174 (2022).
1354 40. J. Wang *et al.*, HLA-DR15 Molecules Jointly Shape an Autoreactive T Cell Repertoire in Multiple
1355 Sclerosis. *Cell* **183**, 1264-1281 e1220 (2020).
1356 41. P. D. Cani, W. M. de Vos, Next-Generation Beneficial Microbes: The Case of Akkermansia
1357 muciniphila. *Front Microbiol* **8**, 1765 (2017).
1358 42. B. Routy *et al.*, Gut microbiome influences efficacy of PD-1-based immunotherapy against epithelial
1359 tumors. *Science* **359**, 91-97 (2018).
1360 43. R. Bhat *et al.*, Inhibitory role for GABA in autoimmune inflammation. *Proc Natl Acad Sci U S A* **107**,
1361 2580-2585 (2010).
1362 44. N. Yalcinkaya *et al.*, Reduced fecal GABA levels in multiple sclerosis patients. *Mult Scler Relat*
1363 *Disord* **9**, 60-61 (2016).
1364 45. N. P. Hyland, J. F. Cryan, A Gut Feeling about GABA: Focus on GABA(B) Receptors. *Front*
1365 *Pharmacol* **1**, 124 (2010).
1366 46. P. Strandwitz *et al.*, GABA-modulating bacteria of the human gut microbiota. *Nat Microbiol* **4**, 396-
1367 403 (2019).
1368 47. K. Z. Coyte, S. Rakoff-Nahoum, Understanding Competition and Cooperation within the Mammalian
1369 Gut Microbiome. *Curr Biol* **29**, R538-R544 (2019).
1370 48. K. Faust *et al.*, Signatures of ecological processes in microbial community time series. *Microbiome* **6**,
1371 120 (2018).
1372 49. A. L. Gould *et al.*, Microbiome interactions shape host fitness. *Proc Natl Acad Sci U S A* **115**, E11951-
1373 E11960 (2018).
1374 50. S. Rakoff-Nahoum, K. R. Foster, L. E. Comstock, The evolution of cooperation within the gut
1375 microbiota. *Nature* **533**, 255-259 (2016).
1376 51. S. F. Henriques *et al.*, Metabolic cross-feeding in imbalanced diets allows gut microbes to improve
1377 reproduction and alter host behaviour. *Nat Commun* **11**, 4236 (2020).
1378 52. C. Yang *et al.*, Fecal IgA Levels Are Determined by Strain-Level Differences in Bacteroides ovatus
1379 and Are Modifiable by Gut Microbiota Manipulation. *Cell Host Microbe* **27**, 467-475 e466 (2020).
1380 53. A. Steimle, M. Neumann, E. T. Grant, J. D. Turner, M. S. Desai, Concentrated Raw Fibers Enhance
1381 the Fiber-Degrading Capacity of a Synthetic Human Gut Microbiome. *Int J Mol Sci* **22**, (2021).

54. J. J. Kozich, S. L. Westcott, N. T. Baxter, S. K. Highlander, P. D. Schloss, Development of a dual-index sequencing strategy and curation pipeline for analyzing amplicon sequence data on the MiSeq Illumina sequencing platform. *Appl Environ Microbiol* **79**, 5112-5120 (2013).
55. P. D. Schloss *et al.*, Introducing mothur: open-source, platform-independent, community-supported software for describing and comparing microbial communities. *Appl Environ Microbiol* **75**, 7537-7541 (2009).
56. A. Steimle, E. T. Grant, M. S. Desai, Quantitative assay to detect bacterial glycan-degrading enzyme activities in mouse and human fecal samples. *STAR Protoc* **2**, 100326 (2021).
57. M. C. Buscarinu *et al.*, Altered intestinal permeability in patients with relapsing-remitting multiple sclerosis: A pilot study. *Mult Scler* **23**, 442-446 (2017).
58. J. D. Glenn, E. M. Mowry, Emerging Concepts on the Gut Microbiome and Multiple Sclerosis. *J Interferon Cytokine Res* **36**, 347-357 (2016).
59. K. Kasahara *et al.*, Interactions between Roseburia intestinalis and diet modulate atherogenesis in a murine model. *Nat Microbiol* **3**, 1461-1471 (2018).
60. G. P. Rodriguez-Castano *et al.*, Bacteroides thetaiotaomicron Starch Utilization Promotes Quercetin Degradation and Butyrate Production by Eubacterium ramulus. *Front Microbiol* **10**, 1145 (2019).
61. A. Haghikia *et al.*, Dietary Fatty Acids Directly Impact Central Nervous System Autoimmunity via the Small Intestine. *Immunity* **43**, 817-829 (2015).

Figure 1

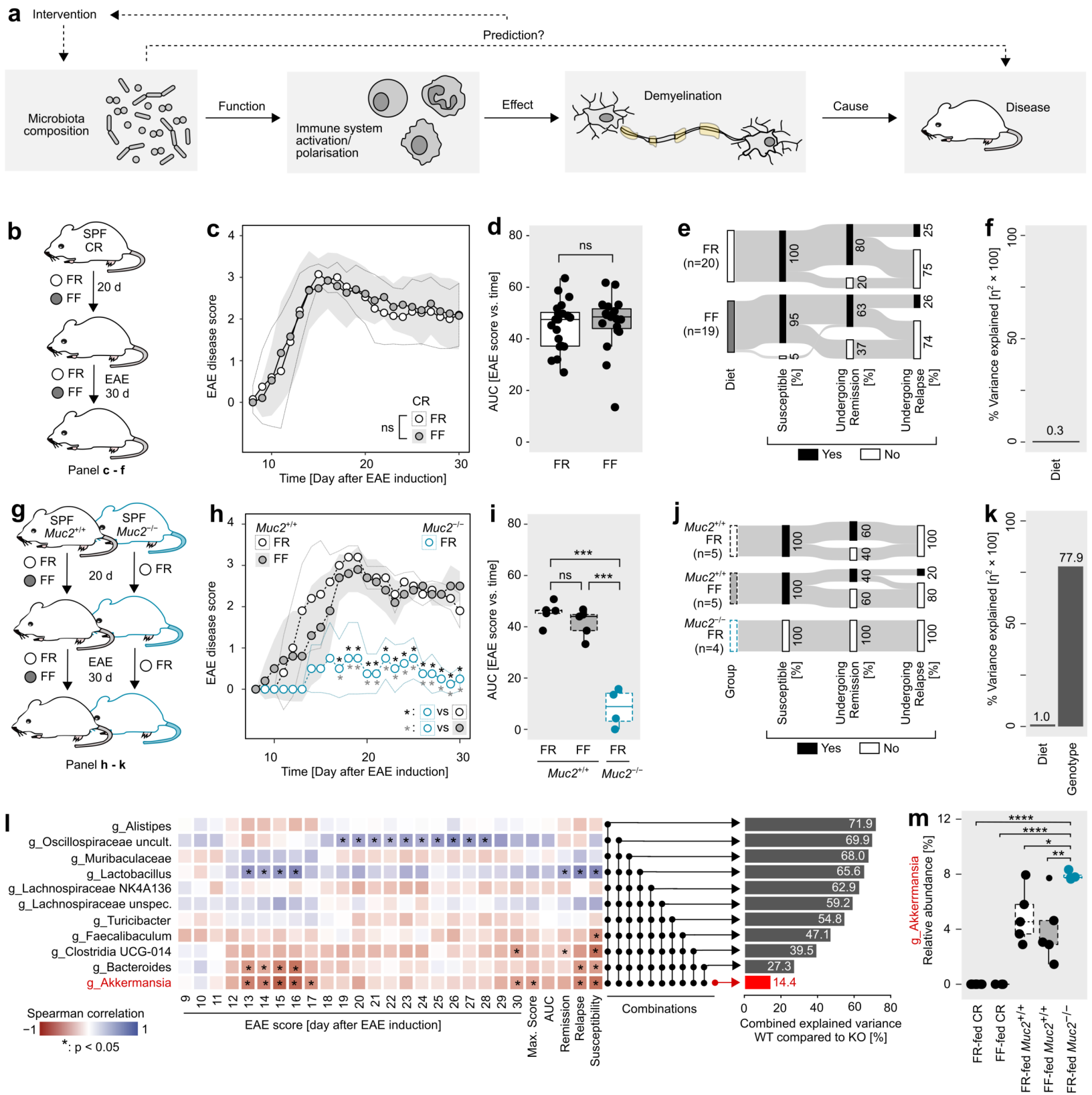
a
Intervention
Prediction?
Microbiota composition
Function
Immune system activation/ polarisation
Effect
Demyelination
Cause
Disease
b
SPF CR
FR
FF
20 d
EAE 30 d
Panel c - f
c
EAE disease score
Time [Day after EAE induction]
CR
ns
FR
FF
d
AUC [EAE score vs. time]
ns
FR
FF
e
FR (n=20)
FF (n=19)
Diet
Susceptible [%]
Undergoing Remission [%]
Undergoing Relapse [%]
Yes
No
f
% Variance explained [η² × 100]
0.3
Diet
g
SPF Muc2+/+
SPF Muc2−/−
20 d
EAE 30 d
Panel h - k
h
Muc2+/+
Muc2−/−
FR
FF
EAE disease score
Time [Day after EAE induction]
vs
i
AUC [EAE score vs. time]
***
ns
***
FR
FF
FR
Muc2+/+
Muc2−/−
j
Muc2+/+ FR (n=5)
Muc2+/+ FF (n=5)
Muc2−/− FR (n=4)
Group
Susceptible [%]
Undergoing Remission [%]
Undergoing Relapse [%]
Yes
No
k
% Variance explained [η² × 100]
1.0
77.9
Diet
Genotype
l
g_Alistipes
g_Oscillospiraceae uncult.
g_Muribaculaceae
g_Lactobacillus
g_Lachnospiraceae NK4A136
g_Lachnospiraceae unspec.
g_Turicibacter
g_Faecalibaculum
g_Clostridia UCG-014
g_Bacteroides
g_Akkermansia
EAE score [day after EAE induction]
Max. Score
AUC
Remission
Relapse
Susceptibility
Combinations
71.9
69.9
68.0
65.6
62.9
59.2
54.8
47.1
39.5
27.3
14.4
Combined explained variance WT compared to KO [%]
Spearman correlation
−1
1
*: p < 0.05
m
g_Akkermansia Relative abundance [%]
FR-fed CR
FF-fed CR
FR-fed Muc2+/+
FF-fed Muc2+/+
FR-fed Muc2−/−

Figure 2

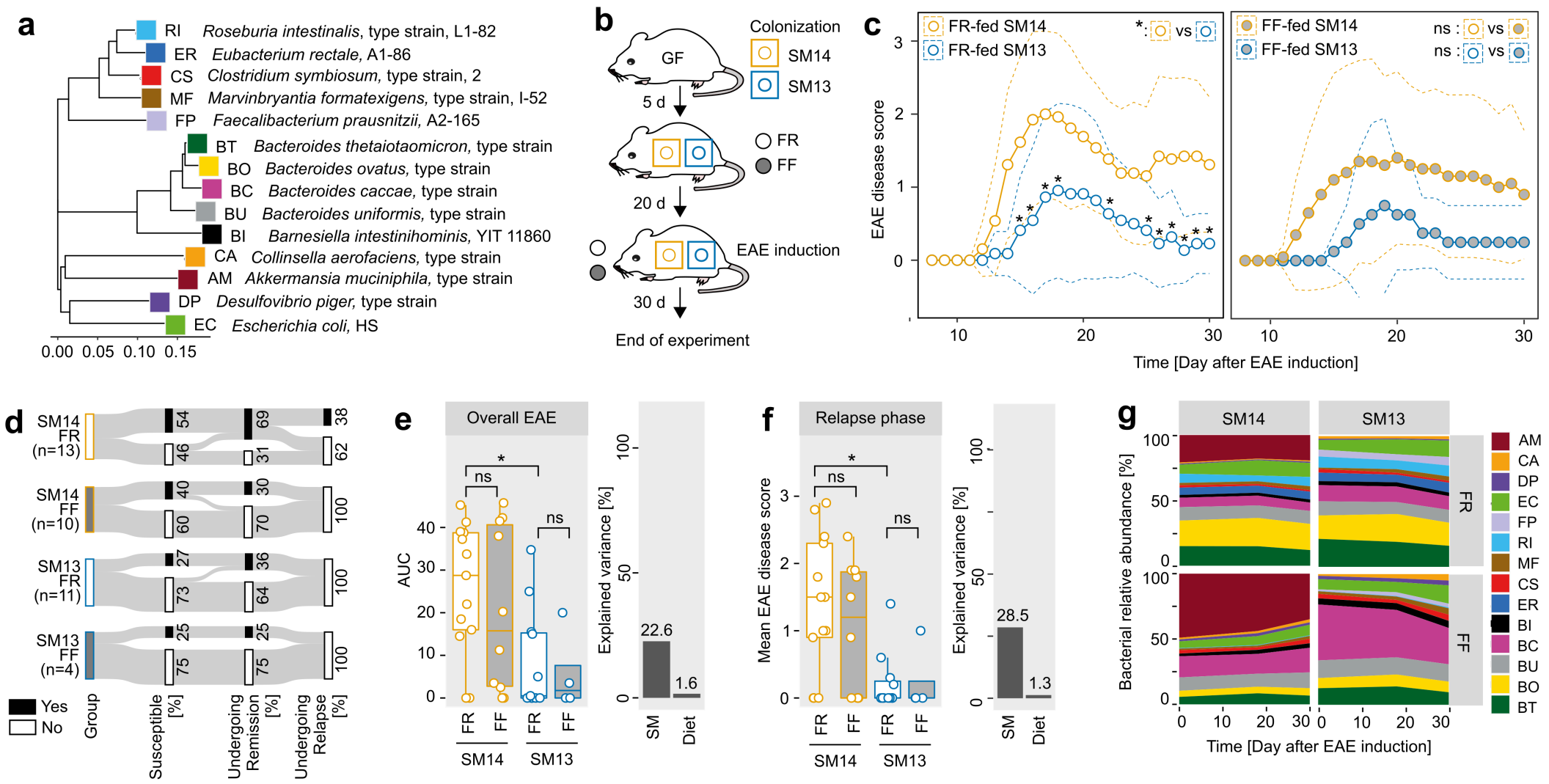
a
RI Roseburia intestinalis, type strain, L1-82
ER Eubacterium rectale, A1-86
CS Clostridium symbiosum, type strain, 2
MF Marvinbryantia formatexigens, type strain, I-52
FP Faecalibacterium prausnitzii, A2-165
BT Bacteroides thetaiotaomicron, type strain
BO Bacteroides ovatus, type strain
BC Bacteroides caccae, type strain
BU Bacteroides uniformis, type strain
BI Barnesiella intestinihominis, YIT 11860
CA Collinsella aerofaciens, type strain
AM Akkermansia muciniphila, type strain
DP Desulfovibrio piger, type strain
EC Escherichia coli, HS
0.00 0.05 0.10 0.15
b
GF
5 d
20 d
30 d
End of experiment
Colonization
SM14
SM13
FR
FF
EAE induction
c
FR-fed SM14
FR-fed SM13
*: vs
FF-fed SM14
FF-fed SM13
ns : vs
EAE disease score
Time [Day after EAE induction]
d
SM14 FR (n=13)
SM14 FF (n=10)
SM13 FR (n=11)
SM13 FF (n=4)
Yes
No
Group
Susceptible [%]
Undergoing Remission [%]
Undergoing Relapse [%]
e
Overall EAE
AUC
ns
*
FR
FF
SM14
SM13
Explained variance [%]
22.6
1.6
SM
Diet
f
Relapse phase
Mean EAE disease score
28.5
1.3
g
SM14
SM13
Bacterial relative abundance [%]
Time [Day after EAE induction]
AM
CA
DP
EC
FP
RI
MF
CS
ER
BI
BC
BU
BO
BT

Figure 3

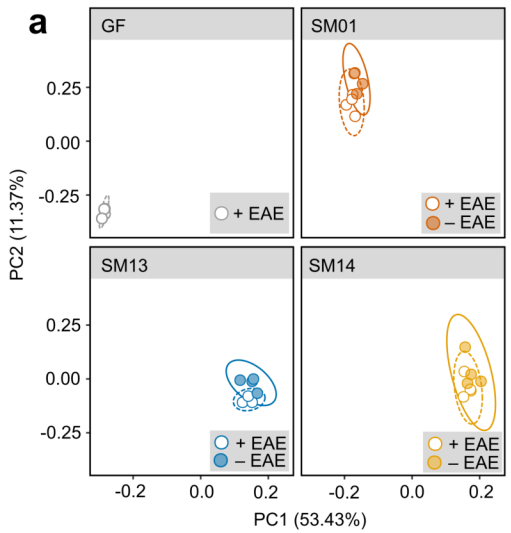
a
GF
SM01
SM13
SM14
+ EAE
– EAE
PC2 (11.37%)
PC1 (53.43%)
0.25
0.00
-0.25
-0.2
0.0
0.2

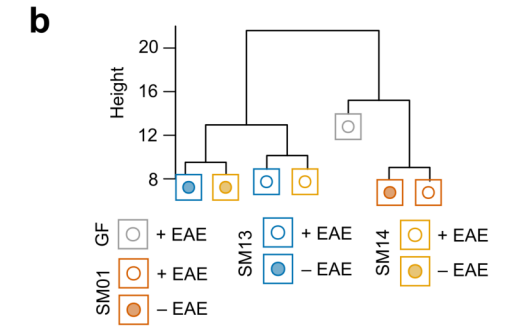
b
Height
20
16
12
8
GF
SM01
SM13
SM14
+ EAE
– EAE

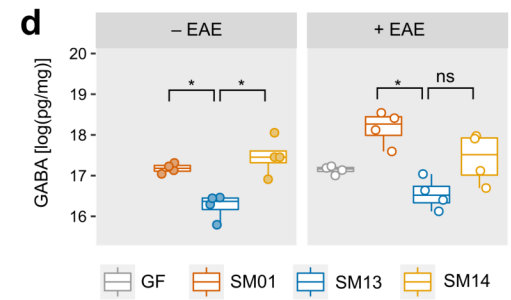
d
– EAE
+ EAE
GABA [log(pg/mg)]]
20
19
18
17
16
*
ns
GF
SM01
SM13
SM14

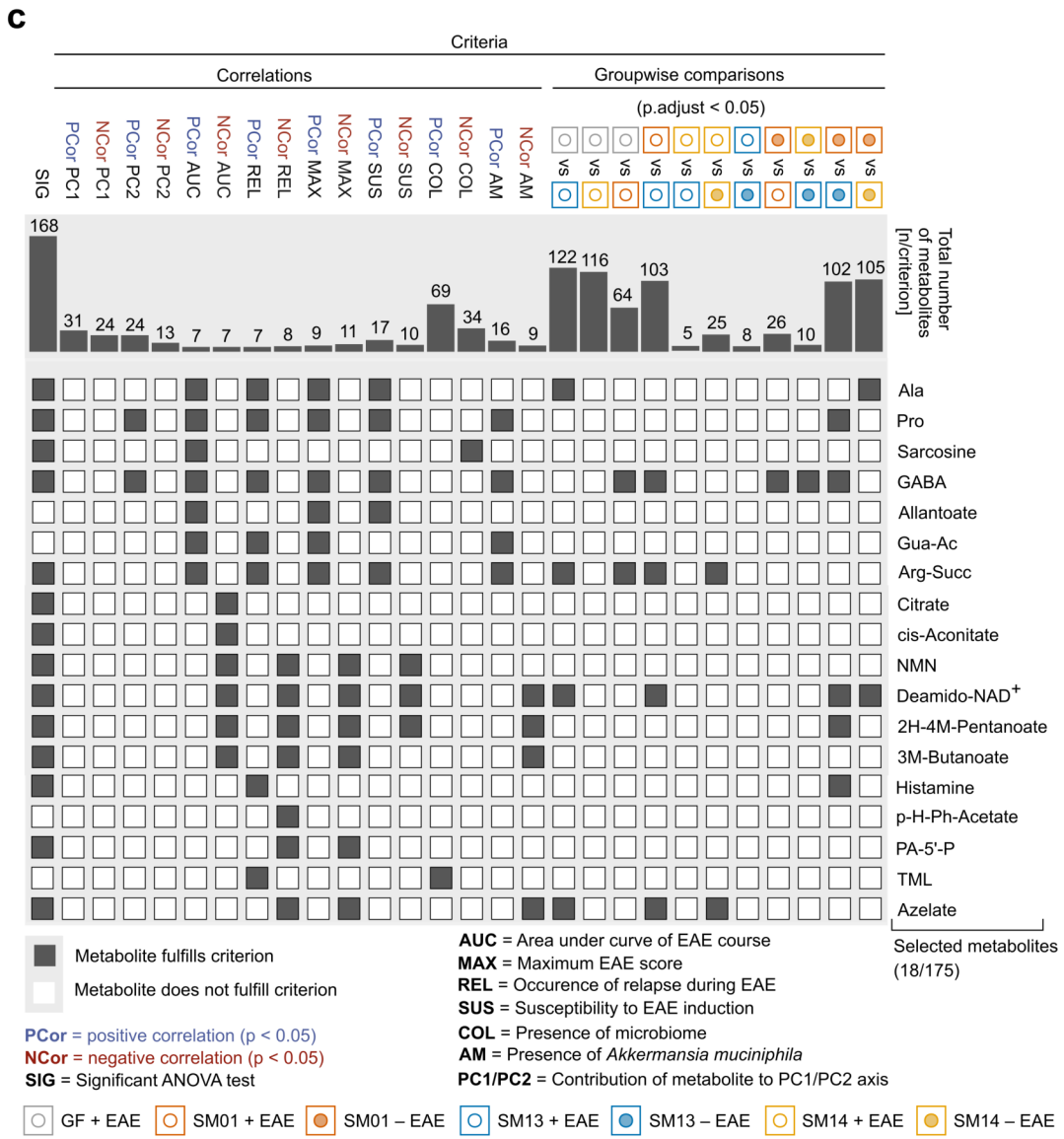
c
Criteria
Correlations
Groupwise comparisons
(p.adjust < 0.05)
SIG
PCor PC1
NCor PC1
PCor PC2
NCor PC2
PCor AUC
NCor AUC
PCor REL
NCor REL
PCor MAX
NCor MAX
PCor SUS
NCor SUS
PCor COL
NCor COL
PCor AM
NCor AM
vs
Total number of metabolites [n/criterion]
168
31
24
24
13
7
7
7
8
9
11
17
10
69
34
16
9
122
116
64
103
5
25
8
26
10
102
105
Ala
Pro
Sarcosine
GABA
Allantoate
Gua-Ac
Arg-Succ
Citrate
cis-Aconitate
NMN
Deamido-NAD+
2H-4M-Pentanoate
3M-Butanoate
Histamine
p-H-Ph-Acetate
PA-5'-P
TML
Azelate
Selected metabolites (18/175)
Metabolite fulfills criterion
Metabolite does not fulfill criterion
PCor = positive correlation (p < 0.05)
NCor = negative correlation (p < 0.05)
SIG = Significant ANOVA test
AUC = Area under curve of EAE course
MAX = Maximum EAE score
REL = Occurence of relapse during EAE
SUS = Susceptibility to EAE induction
COL = Presence of microbiome
AM = Presence of Akkermansia muciniphila
PC1/PC2 = Contribution of metabolite to PC1/PC2 axis
GF + EAE
SM01 + EAE
SM01 – EAE
SM13 + EAE
SM13 – EAE
SM14 + EAE
SM14 – EAE

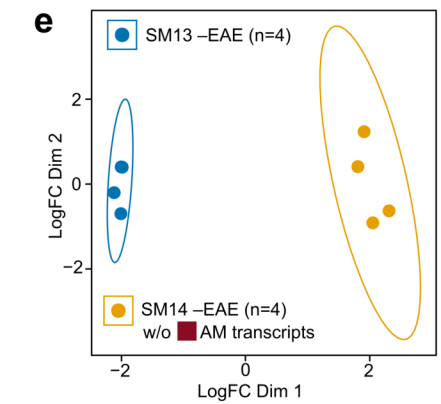
e
SM13 –EAE (n=4)
SM14 –EAE (n=4)
w/o AM transcripts
LogFC Dim 2
LogFC Dim 1
2
0
−2

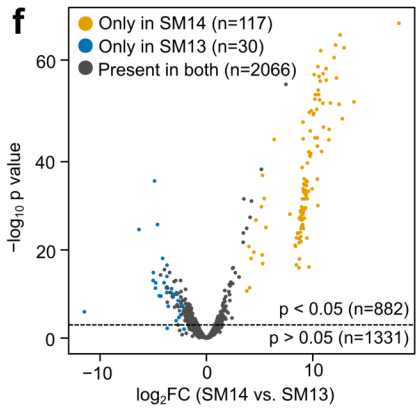
f
Only in SM14 (n=117)
Only in SM13 (n=30)
Present in both (n=2066)
p < 0.05 (n=882)
p > 0.05 (n=1331)
−log10 p value
log2FC (SM14 vs. SM13)
60
40
20
0
−10
0
10

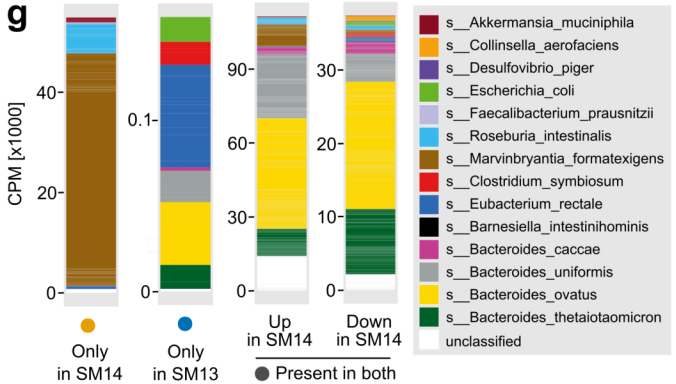
g
CPM [x1000]
Only in SM14
Only in SM13
Up in SM14
Down in SM14
Present in both
s__Akkermansia_muciniphila
s__Collinsella_aerofaciens
s__Desulfovibrio_piger
s__Escherichia_coli
s__Faecalibacterium_prausnitzii
s__Roseburia_intestinalis
s__Marvinbryantia_formatexigens
s__Clostridium_symbiosum
s__Eubacterium_rectale
s__Barnesiella_intestinihominis
s__Bacteroides_caccae
s__Bacteroides_uniformis
s__Bacteroides_ovatus
s__Bacteroides_thetaiotaomicron
unclassified

Figure 4

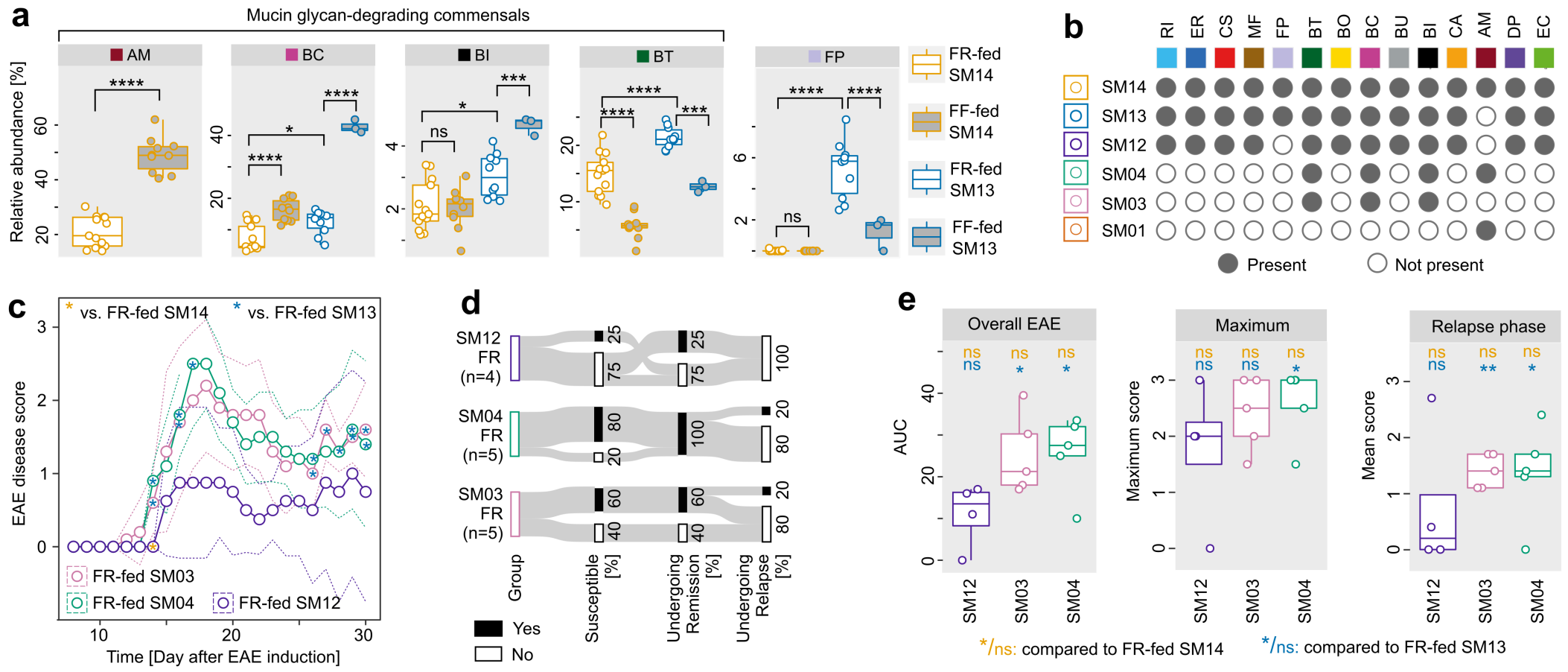
a
Mucin glycan-degrading commensals
AM
BC
BI
BT
FP
Relative abundance [%]
FR-fed SM14
FF-fed SM14
FR-fed SM13
FF-fed SM13
b
RI ER CS MF FP BT BO BC BU BI CA AM DP EC
SM14
SM13
SM12
SM04
SM03
SM01
Present
Not present
c
vs. FR-fed SM14
vs. FR-fed SM13
EAE disease score
FR-fed SM03
FR-fed SM04
FR-fed SM12
Time [Day after EAE induction]
d
SM12 FR (n=4)
SM04 FR (n=5)
SM03 FR (n=5)
Group
Susceptible [%]
Undergoing Remission [%]
Undergoing Relapse [%]
Yes
No
e
Overall EAE
Maximum
Relapse phase
AUC
Maximum score
Mean score
SM12
SM03
SM04
*/ns: compared to FR-fed SM14
*/ns: compared to FR-fed SM13

Figure 5

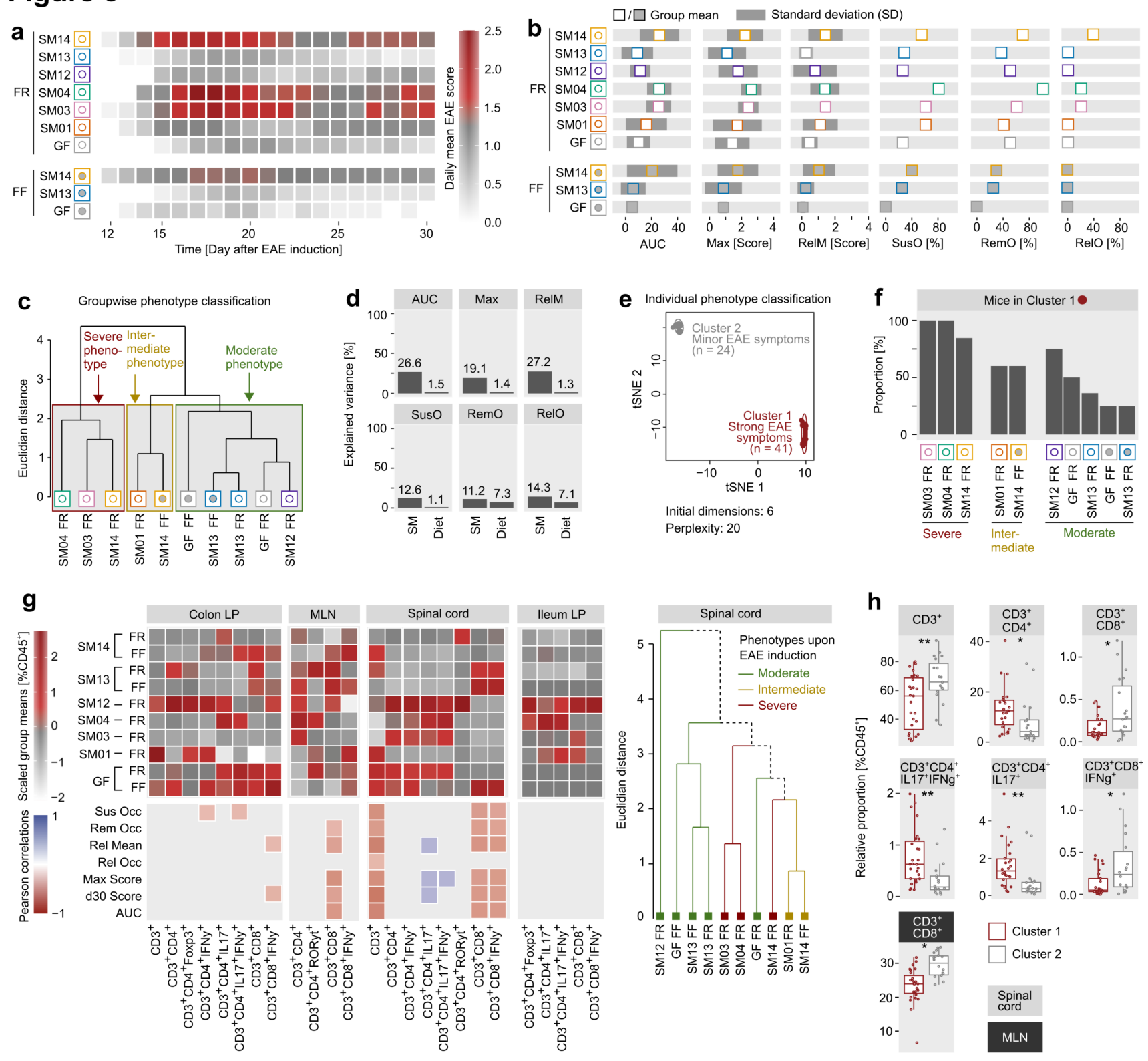
a
FR
SM14
SM13
SM12
SM04
SM03
SM01
GF
FF
SM14
SM13
GF
Daily mean EAE score
Time [Day after EAE induction]
b
Group mean
Standard deviation (SD)
AUC
Max [Score]
RelM [Score]
SusO [%]
RemO [%]
RelO [%]
c
Groupwise phenotype classification
Severe phenotype
Intermediate phenotype
Moderate phenotype
Euclidian distance
SM04 FR
SM03 FR
SM14 FR
SM01 FR
SM14 FF
GF FF
SM13 FF
SM13 FR
GF FR
SM12 FR
d
AUC
Max
RelM
SusO
RemO
RelO
Explained variance [%]
26.6
1.5
19.1
1.4
27.2
1.3
12.6
1.1
11.2
7.3
14.3
7.1
SM
Diet
e
Individual phenotype classification
Cluster 2
Minor EAE symptoms
(n = 24)
Cluster 1
Strong EAE symptoms
(n = 41)
tSNE 1
tSNE 2
Initial dimensions: 6
Perplexity: 20
f
Mice in Cluster 1
Proportion [%]
SM03 FR
SM04 FR
SM14 FR
SM01 FR
SM14 FF
SM12 FR
GF FR
SM13 FR
GF FF
SM13 FR
Severe
Inter-mediate
Moderate
g
Colon LP
MLN
Spinal cord
Ileum LP
Scaled group means [%CD45+]
Pearson correlations
Sus Occ
Rem Occ
Rel Mean
Rel Occ
Max Score
d30 Score
AUC
Spinal cord
Phenotypes upon EAE induction
Moderate
Intermediate
Severe
Euclidian distance
h
CD3+
CD3+ CD4+
CD3+ CD8+
CD3+CD4+ IL17+IFNg+
CD3+CD4+ IL17+
CD3+CD8+ IFNg+
Relative proportion [%CD45+]
Cluster 1
Cluster 2
Spinal cord
MLN

Figure 6

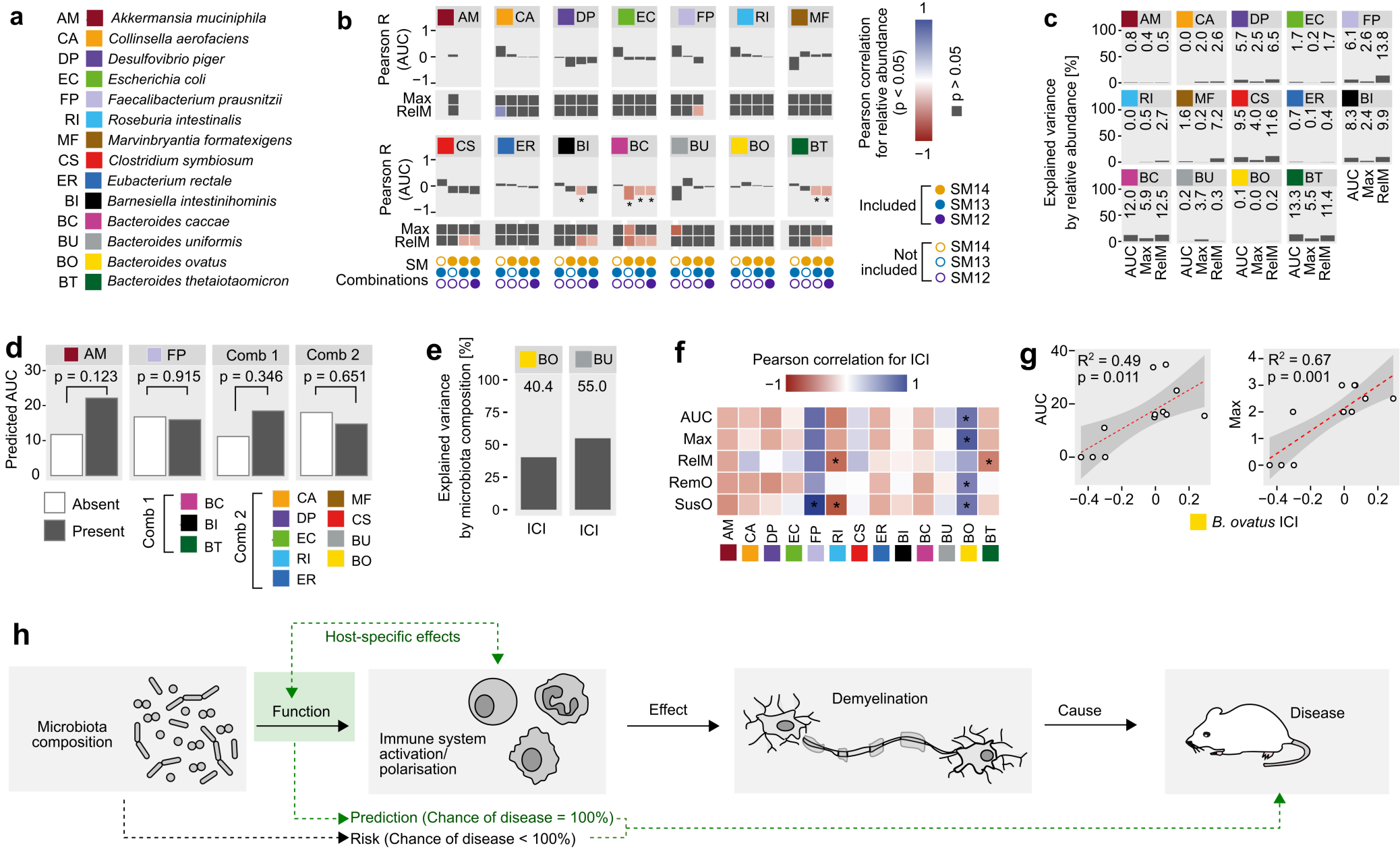
a
AM Akkermansia muciniphila
CA Collinsella aerofaciens
DP Desulfovibrio piger
EC Escherichia coli
FP Faecalibacterium prausnitzii
RI Roseburia intestinalis
MF Marvinbryantia formatexigens
CS Clostridium symbiosum
ER Eubacterium rectale
BI Barnesiella intestinihominis
BC Bacteroides caccae
BU Bacteroides uniformis
BO Bacteroides ovatus
BT Bacteroides thetaiotaomicron
b
Pearson R (AUC)
Max RelM
SM Combinations
Pearson correlation for relative abundance (p < 0.05)
p > 0.05
Included SM14 SM13 SM12
Not included SM14 SM13 SM12
c
Explained variance by relative abundance [%]
AUC Max RelM
d
Predicted AUC
p = 0.123
p = 0.915
p = 0.346
p = 0.651
Absent
Present
Comb 1 BC BI BT
Comb 2 CA DP EC RI ER MF CS BU BO
e
Explained variance by microbiota composition [%]
BO 40.4
BU 55.0
ICI
f
Pearson correlation for ICI
AUC Max RelM RemO SusO
g
R² = 0.49 p = 0.011
R² = 0.67 p = 0.001
B. ovatus ICI
h
Host-specific effects
Microbiota composition
Function
Immune system activation/ polarisation
Effect
Demyelination
Cause
Disease
Prediction (Chance of disease = 100%)
Risk (Chance of disease < 100%)

Extended Data Figure 1

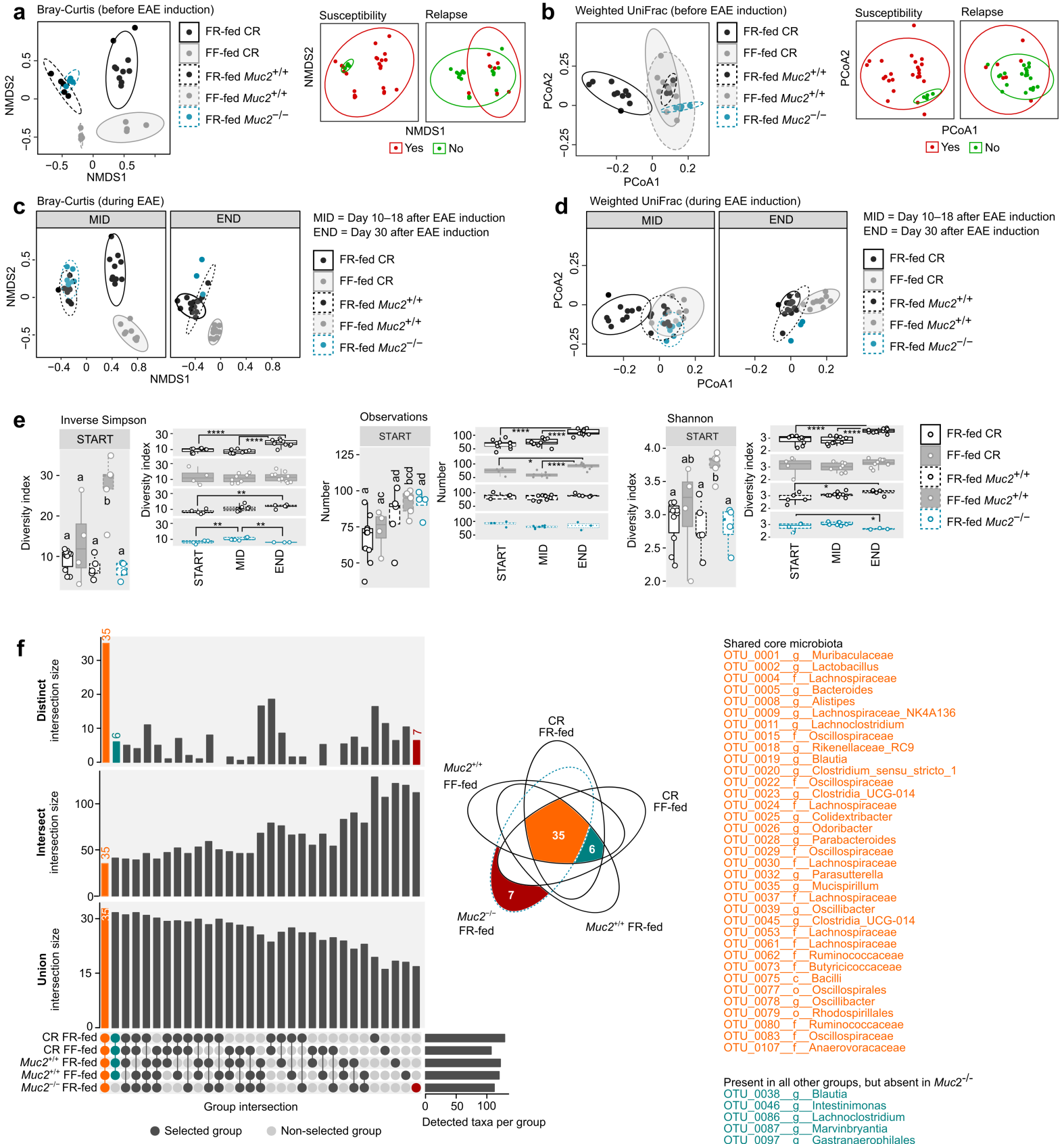

Extended Data Figure 2

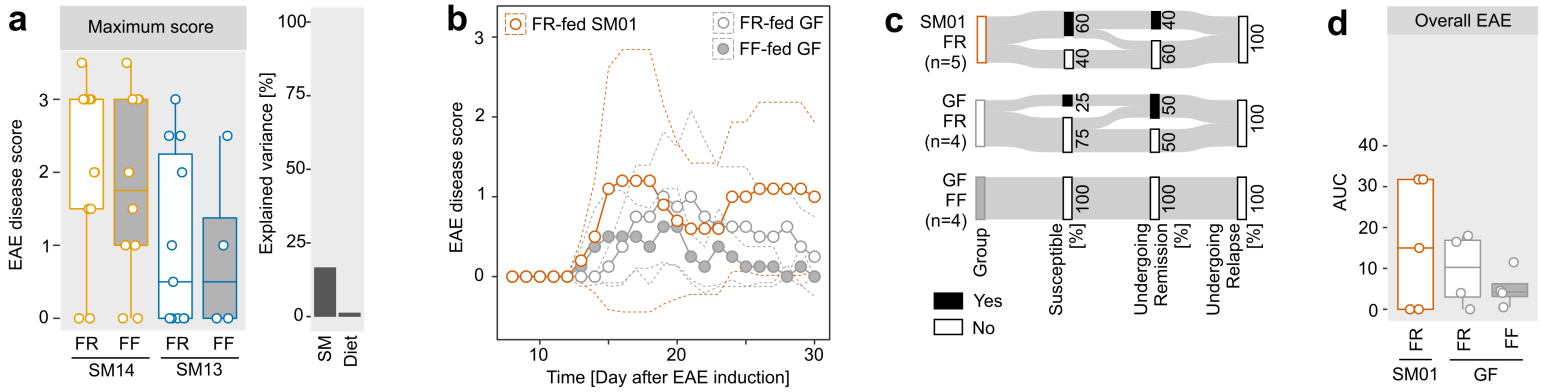

Extended Data Figure 3

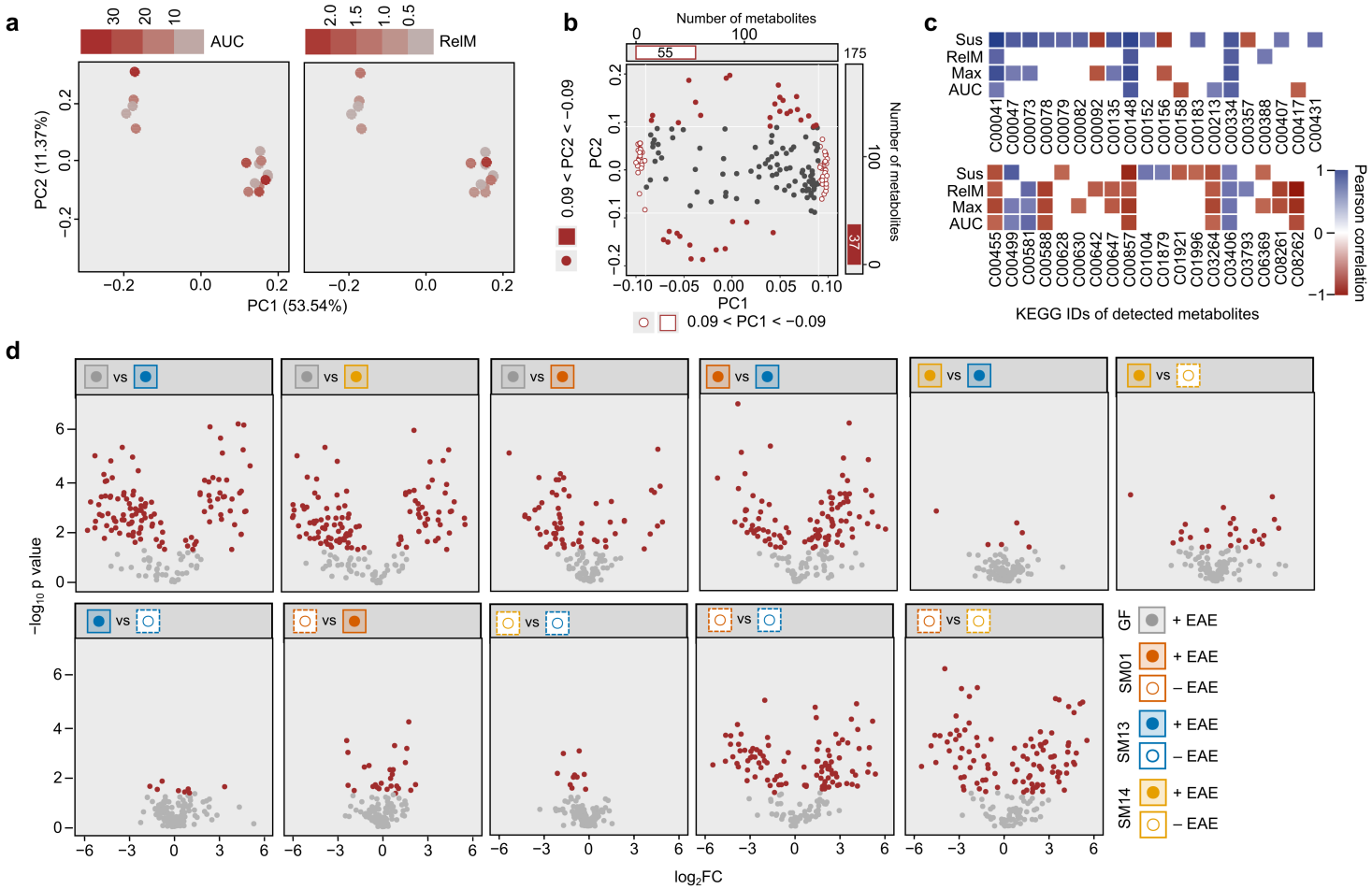

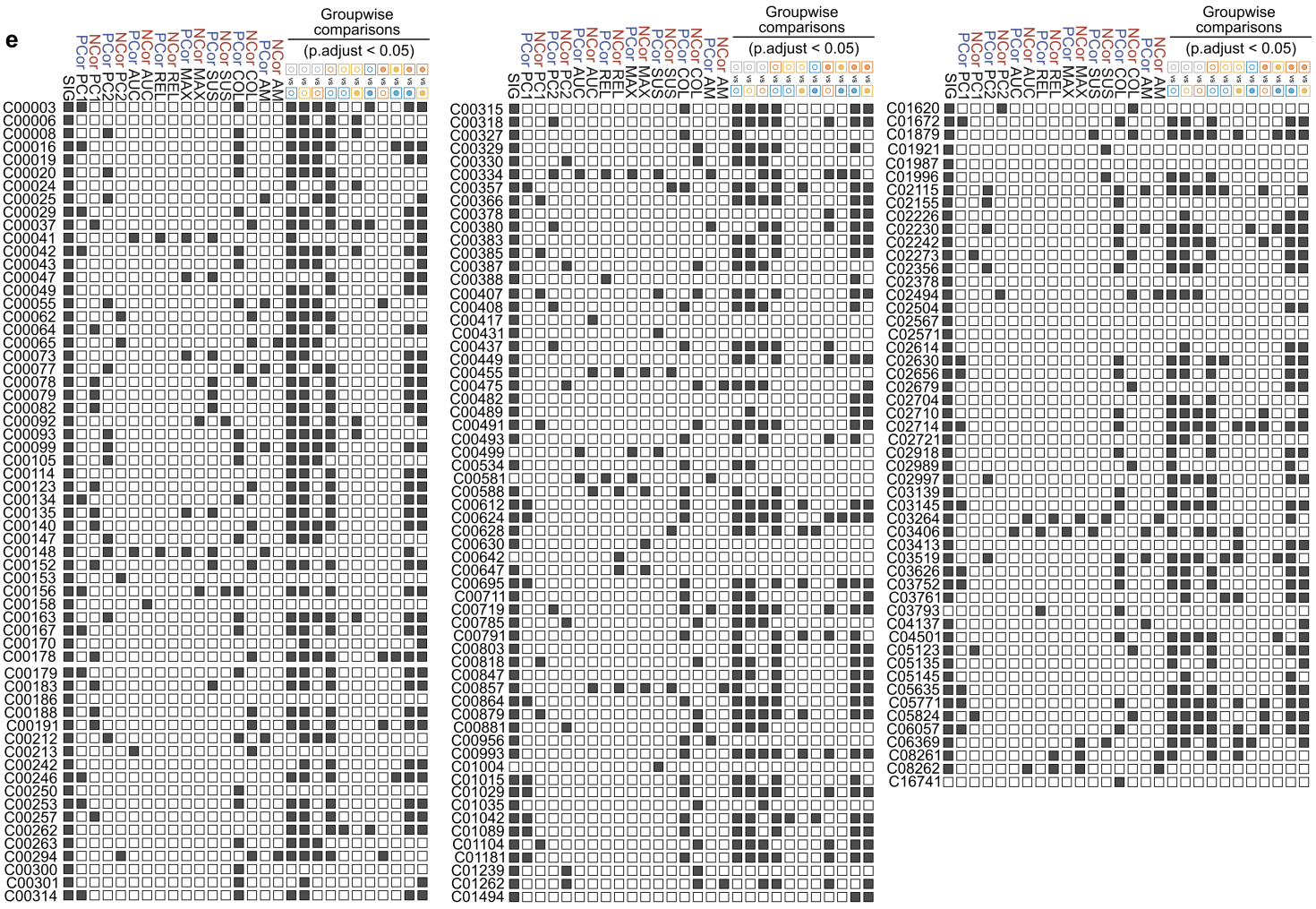

Extended Data Figure 4

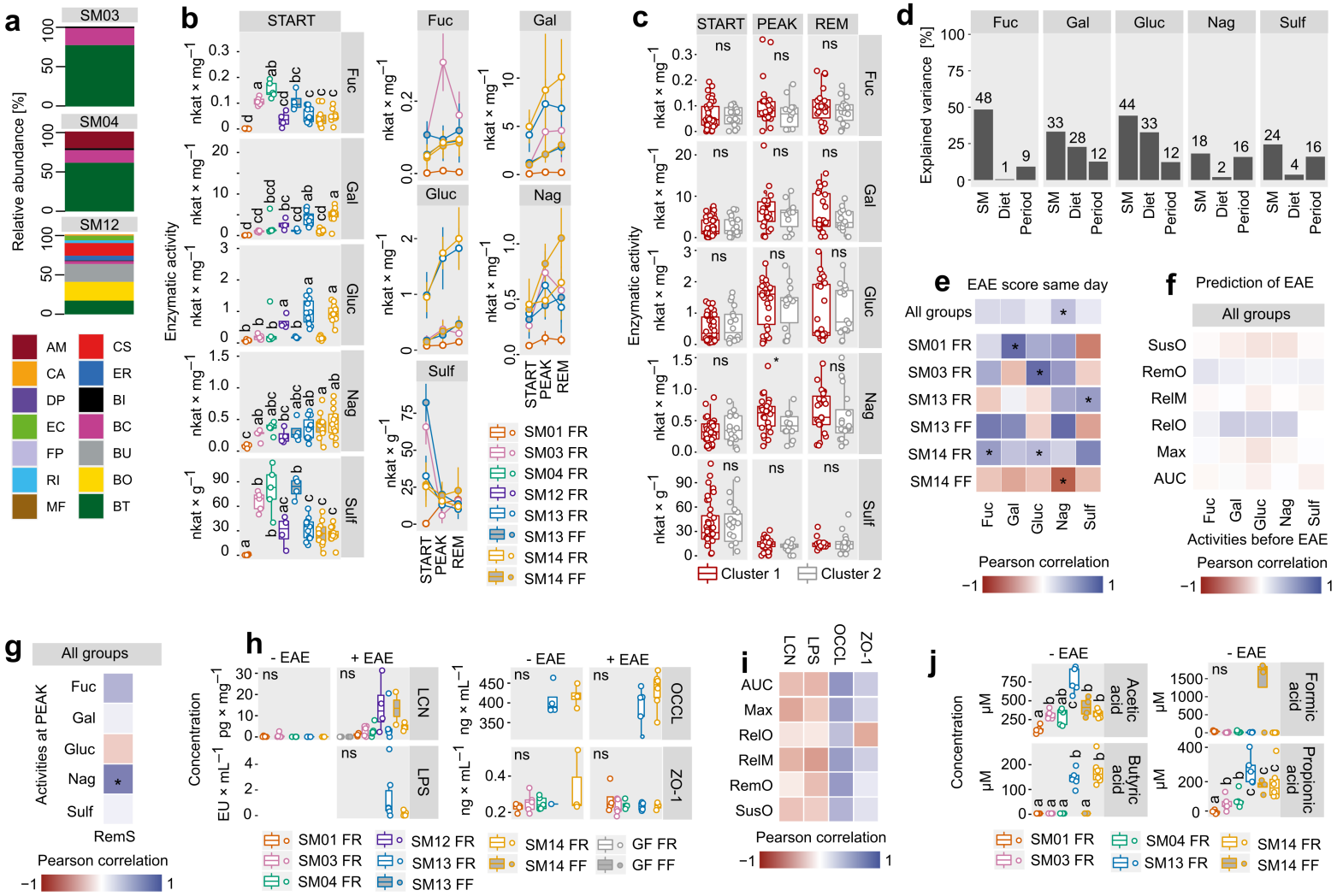

Extended Data Figure 5

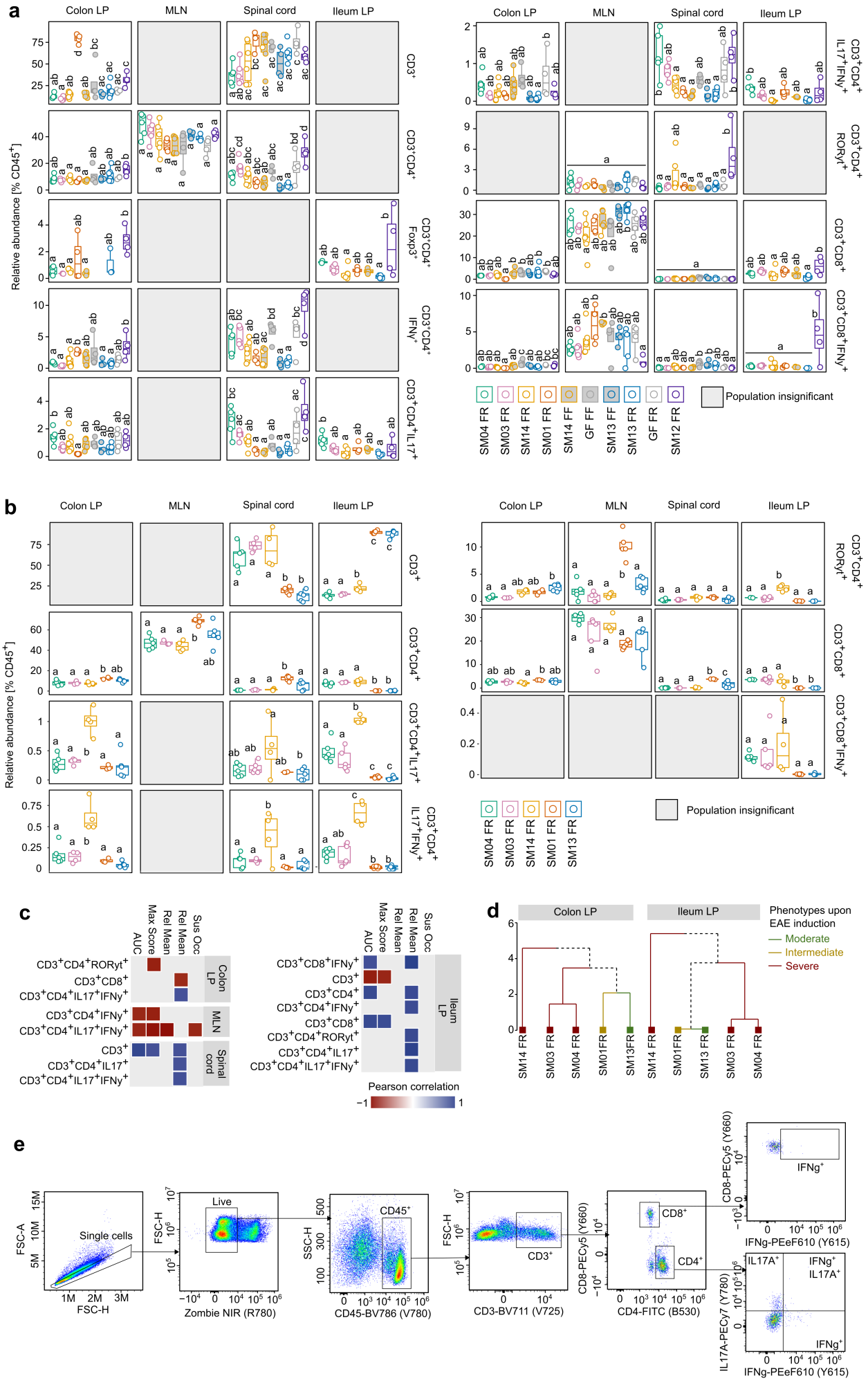

Extended Data Figure 6

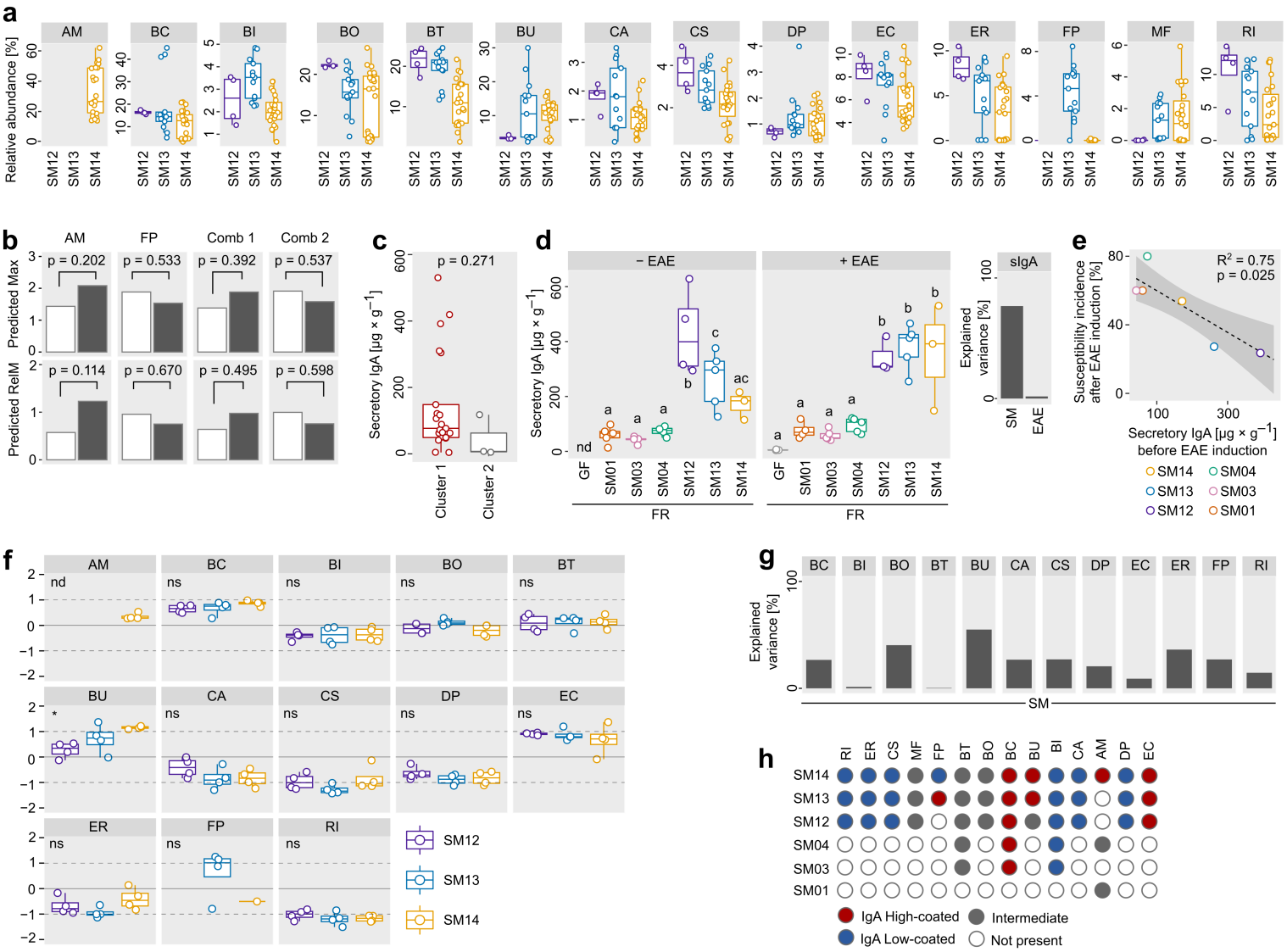

ICI

Extended Data Figure 7

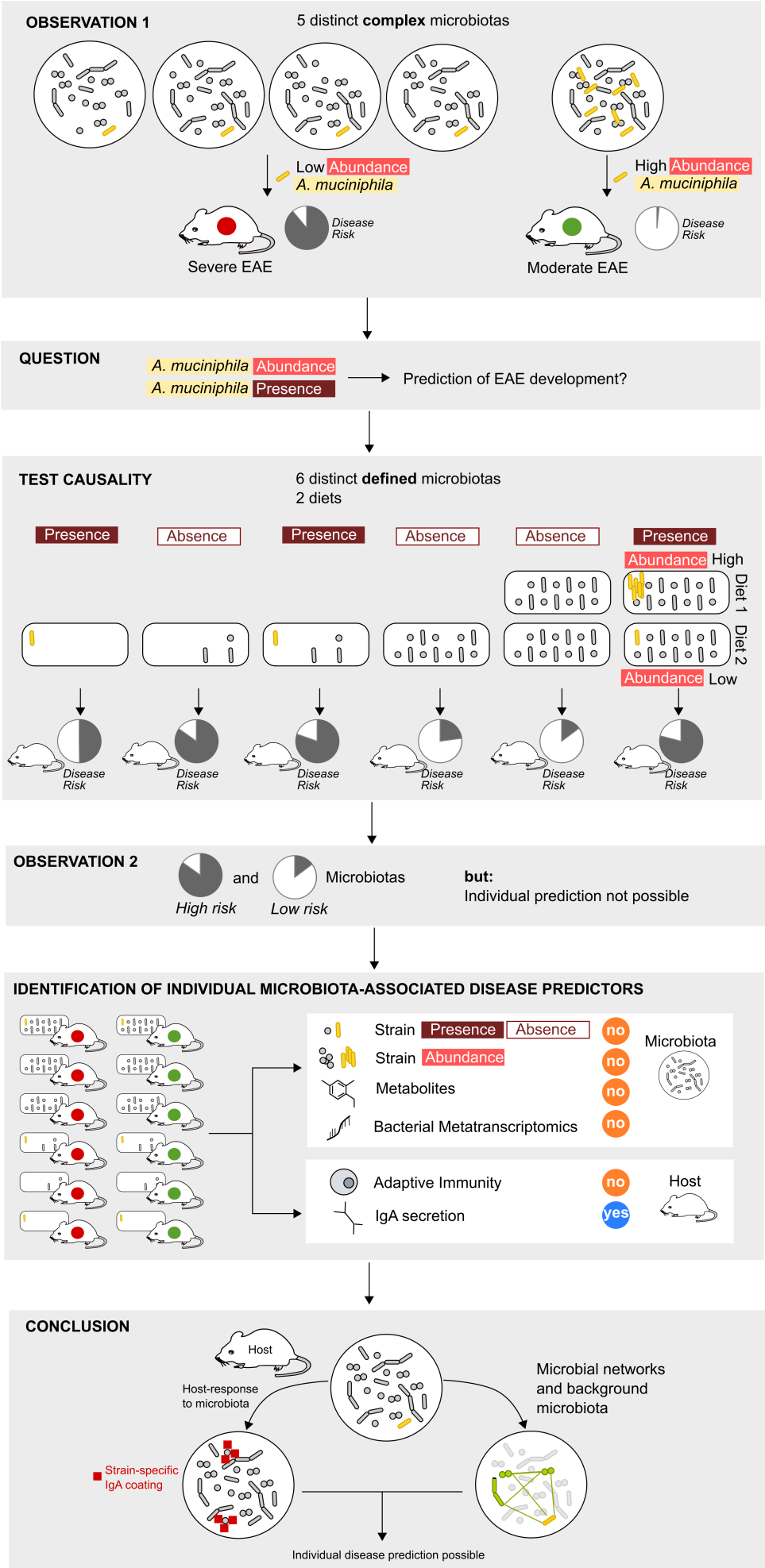
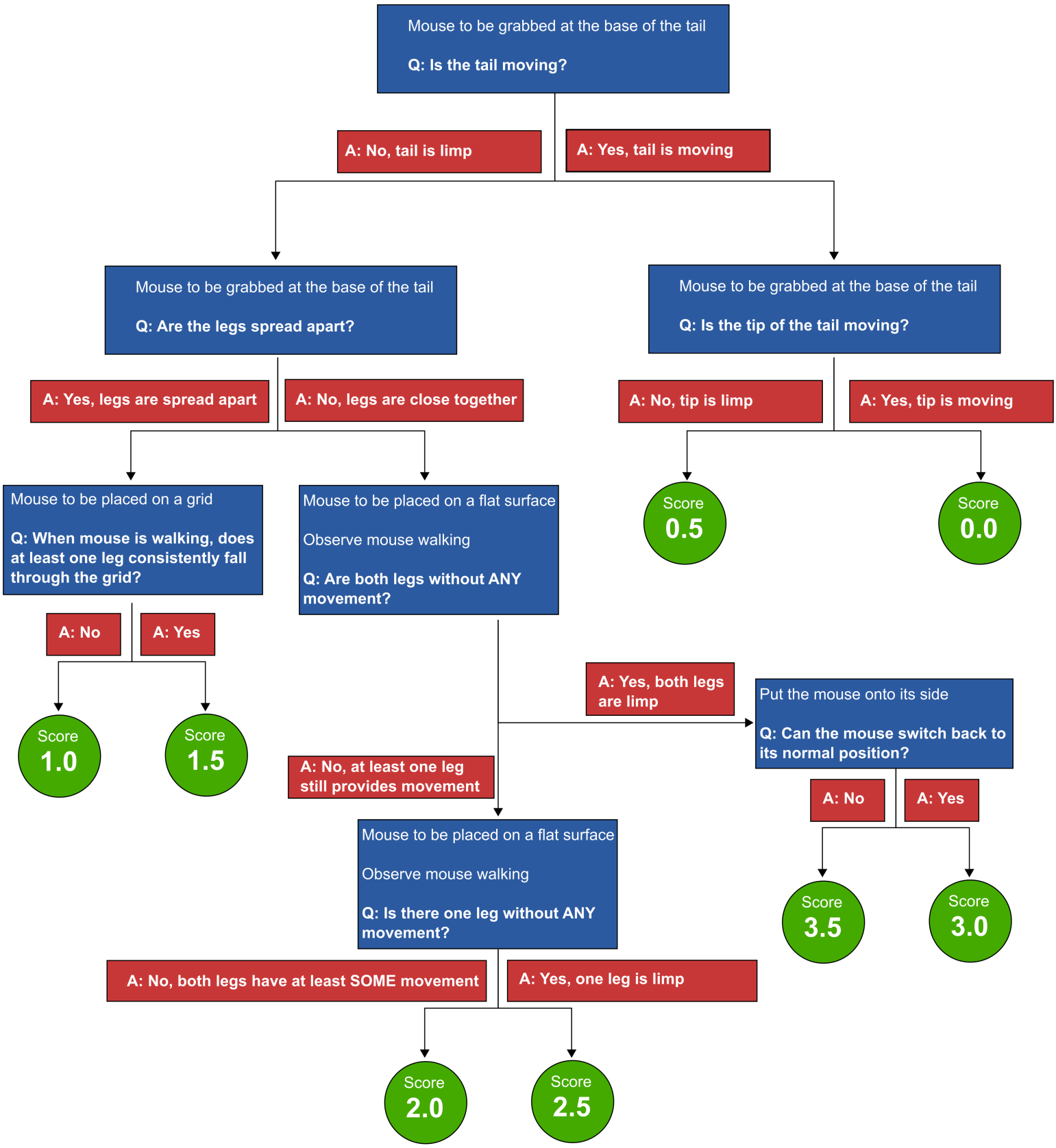
Extended Data Figure 8